Thermal signature of the Majorana fermion in a Josephson junction

Aabir Mukhopadhyay* and Sourin Das†
Indian Institute of Science Education and Research Kolkata, Mohanpur, Nadia 741 246, West Bengal, India

(Received 26 February 2020; revised 2 March 2021; accepted 2 March 2021; published 5 April 2021)

Possible signatures of "Majorana end states" are discussed by combining information extracted from subgap Cooper pair transport and transport of heat by excited quasiparticles above the gap across a thermally biased Josephson junction setup formed out of a one-dimensional (1D) topological superconductor hosting Majorana end states. We show that the presence of Majorana end states results in two sets of testable relations: (i) the ratios between the various multiterminal thermal conductances is independent of the Josephson phase bias, and (ii) the phase independence of the ratios of "ratios of the phase derivative of multiterminal thermal conductance and the corresponding Josephson current", in a three-terminal setup. We contrast out findings with a Josephson junction setup composed of a 1D topological superconductor hosting "Andreev type end states" and show that they violate the above-mentioned relations. We also discuss how the presence of nonequilibrium noise in thermal current influences our predictions.

DOI: 10.1103/PhysRevB.103.144502

I. INTRODUCTION

Maki and Griffin [1,2] carried out a theoretical study of heat transport across a Josephson junction in 1965 and since then there have been several studies pertaining to thermal transport across Josephson junctions [3–7] including some recent developments involving two- and three-dimensional topological insulators [8,9]. On the experimental side, the theoretical predictions [1,2] were confirmed in a remarkable experiment by Giazotto and Martínez-Pérez in 2012 [10] which led to steady experimental progress in this field [11–22].

Proximity-induced superconductivity in spin-orbit nanowire and the helical edge state of quantum spin Hall [23] state allow for two distinct realizations of topological superconductivity and localized Majorana end states (MESs) [24–37]. In the case of a nanowire, these MESs are expected to appear at the two ends of the wire [38] while for helical edge state of the quantum spin Hall state, localized MESs form at the junction of a proximity-induced superconducting region and a region exposed to the Zeeman field [39,40]. It is pertinent to note that experimental realization of Josephson junctions of one-dimensional (1D) topological superconductors hosting Majorana end states has been achieved both in the context of nanowire setup [41] and the helical edge state of a quantum spin Hall state setup [42]. These experimental advances call for a renewed look at how to exploit a combination of electrical and thermal means to detect and manipulate the MES.

As far as the detection of MESs via the Josephson effect is concerned, observation of the 4π Josephson effect [39,43] is considered as one of the hallmarks of MESs which primarily relates to subgap physics. The central focus of this paper is to establish that the above-gap transport of thermally excited bulk quasiparticles across a Josephson junction also carries distinctive signatures of MESs. This can be understood as follows.

It is known that the thermal current across a Josephson junction in the weak tunneling limit can be expressed as a sum of contribution due to quasiparticle tunneling, Cooper pairs tunneling (which is usually negligible [44]), and the interference of the two [1,2,45]. For a Josephson junction with arbitrary transparency, these interferences simply lead to zero in the denominator of transmission probability of quasiparticles at energies (denoted by ω_0) at which Andreev bound states [46–49] are formed in the Josephson junction. Remarkably, the phase bias (ϕ) of the Josephson junctions of 1D topological superconductor hosting Majorana end states (we name these junctions as Majorana-Josephson junction) enters the quasiparticle transmission probability solely via the dependence of subgap bound states energy [$\omega_0(\phi)$] on ϕ which is very distinct from the ϕ dependence of the transmission probability of the non-Majorana 1D Josephson junction (see Appendix A and Sec. IV E) irrespective of the fact that they are topological [50] or nontopological [4]. Now we recall that the Josephson current is dominated by contributions from the ϕ derivative of the subgap bound state energy, $\omega_0(\phi)$, in the short junction limit [47]. Hence, both the heat current carried by the thermally excited quasiparticles and Josephson current carried by Cooper pairs acquire their ϕ dependence primarily from the dependence of ω_0 on ϕ for the Majorana-Josephson junction. This fact should lead to a distinctive correlation between these two independently measurable quantities when measured simultaneously as a function of ϕ. A distinctive correlation between the Josephson current and the heat current is also expected as a function of the normal-state transmission probability (τ) of the Josephson junction owing to the dependence of subgap bound state energy (ω_0) on τ.

*aabir.riku@gmail.com
†sourin@iiserkol.ac.in

In what follows, we study the correlation between Josephson current, thermal conductance, and the corresponding normal-state electrical conductance of a thermally biased three-terminal Majorana-Josephson junction as a function of (ϕ, τ) in the short junction limit. We derive a set of relations [see Eqs. (31) and (32)] between them, which is unique to the 1D Majorana-Josephson junction. We show that the validity of these relations owes its existence to the presence of MESs at the junction and hence can be employed for extracting the smoking gun signature of MESs. We point out that the three-terminal topological Josephson junction setup [51,52] is expected to host a single MES pinned at zero energy [53] and therefore is of particular importance as a testing ground for our theoretical study.

The paper is organized as follows: In Sec. II we define the thermal conductance matrix $(\kappa_{n,m})$ for the multiterminal Josephson junction. In Sec. III we discuss the thermal conductance of the two-terminal Majorana-Josephson junction and signatures of MESs and also point out the possibility of other topological bound states mimicking such signatures. In Sec. IV we study the thermal conductance of the three-terminal Majorana-Josephson junction and establish the relation given in Eqs. (31) and (32), which are the central results of this paper. In Sec. IV D we show that these results are violated as we move away form the short junction limit. Then in Sec. IV E we demonstrate that the results of Eqs. (31) and (32) cannot be mimicked by other topological non-Majorana end states discussed in Ref. [50]. Then in Sec. IV F we demonstrate the degree of deviation for our prediction when the Majorana-Josephson trijunction in the short junction limit is replaced by a trijunction of nontopological 1D superconductors in the short junction limit. In Sec. V we discuss how noise in thermal currents could challenge the verification of Eqs. (31) and (32) and map out the optimal parameter regime supporting large suppression of noise. In Sec. VI we conclude with a discussion on the advantages, disadvantages, and differences of our proposal over other known signatures of MES, such as the 4π Josephson effect, the quantized Majorana conductance, and the zero-bias peak experiments.

II. MULTITERMINAL THERMAL CONDUCTANCE

For a multiterminal junction, heat currents driven by temperature bias within linear response theory can be expressed as

$$I_n^H = \sum_{m\neq n} \kappa_{n,m}(T_n - T_m), \tag{1}$$

where $\kappa_{n,m}$ is the thermal conductance between terminals m and n and T_n, T_m are the temperatures of terminals n and m, respectively. We consider a general multiterminal junction of superconducting leads (described by a Bogoliubov–de Gennes Hamiltonian [54]) connected via a common normal region. An incident electronlike quasiparticle in mth lead (with energy ω) results in a reflected electronlike and holelike quasiparticle within the same lead with probabilities, say $\mathcal{R}_{e,e}^{m,m}$ and $\mathcal{R}_{h,e}^{m,m}$, respectively, along with transmitted electronlike and holelike quasiparticles in the nth lead $(n \neq m)$ with probabilities $\mathcal{T}_{e,e}^{n,m}$ and $\mathcal{T}_{h,e}^{n,m}$, respectively. Probability conservation ensures that $(\mathcal{R}_{e,e}^{m,m} + \mathcal{R}_{h,e}^{m,m}) + \sum_n (\mathcal{T}_{e,e}^{n,m} + \mathcal{T}_{h,e}^{n,m}) = 1$. We denote $\mathcal{T}^{n,m} = \mathcal{T}_e^{n,m} + \mathcal{T}_h^{n,m} = (\mathcal{T}_{e,e}^{n,m} + \mathcal{T}_{h,e}^{n,m}) + (\mathcal{T}_{h,h}^{n,m} + \mathcal{T}_{e,h}^{n,m})$. The multiterminal linear response thermal conductance between leads m and n is then given by [8]

$$\kappa_{n,m}(\phi_j) = \left[\frac{1}{h}\int_{\Delta_0}^{\infty} d\omega\, \omega\, \{\mathcal{T}^{n,m}\} \frac{df(\omega, T)}{dT}\right]_{T=T_{\rm avg}}, \tag{2}$$

where $f(\omega, T)$ is the Fermi distribution function at temperature T, Δ_0 is the superconducting gap (taken to be the same of all leads), and $T_{\rm avg}$ is the average junction temperature.

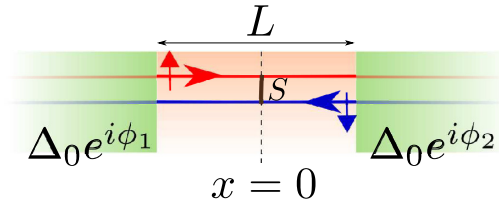

FIG. 1. Pictorial representation of two-terminal Josephson junction hosted on a helical edge state where a backscatterer S is introduced at $x = 0$.

III. TWO-TERMINAL MAJORANA-JOSEPHSON JUNCTION IN HELICAL EDGE STATE

A. The model

We consider a Josephson junction in helical edge state where the junction is defined by an $|x| < L/2$ region and we have a finite pair potential $\Delta_0 e^{i\phi_r}$ ($[r \in \{1, 2\}]$) for $\infty > |x| > L/2$ (see Fig. 1). Our setup is described by a Bogoliubov–de Gennes (BdG) Hamiltonian [39,55] in the Nambu basis $(\Psi = [(\psi_\uparrow, \psi_\downarrow), (\psi_\downarrow^\dagger, -\psi_\uparrow^\dagger)]^T)$ [56] given by

$$\mathcal{H} = (v_F \hat{p}_x \sigma_z - \mu)\tau_z + \Delta(x)(\cos\phi_r \tau_x - \sin\phi_r \tau_y), \tag{3}$$

where $\Delta(x) = \Delta_0[\Theta(-x - L/2) + \Theta(x - L/2)]$, and σ and τ represent spin and particle-hole degrees of freedom, respectively. We focus on the highly doped regime given by the chemical potential $\mu \gg \Delta_0$ and at the short junction limit given by $L \ll \xi$, where $\xi = \hbar v_F/\Delta_0$ is the superconducting coherence length. We also assume a scattering matrix (for the electron) at $x = 0$, given by

$$S^e = \begin{pmatrix} r_{11} & t \\ t & r_{22} \end{pmatrix}. \tag{4}$$

Here r_{ii} represents the amplitude of back-reflection within the terminal i and t represents the amplitude of transmission. The scattering matrix S^e is taken to be symmetric, which ensures that there is no time-reversal breaking phase leading to anomalous Josephson effect. For simplicity, the matrix elements of S^e are assumed to be energy independent.

For energy $\omega < \Delta_0$ (measured with respect to μ), the condition for the formation of an Andreev bound state is given by [47,57]

$$\det[\mathbb{I} - a^2(\omega) S^e e^{i\Phi} S^h e^{-i\Phi}] = 0, \tag{5}$$

where the scattering matrix for hole is given by

$$S^h = \begin{pmatrix} -r_{11}^* & t^* \\ t^* & -r_{22}^* \end{pmatrix} \tag{6}$$

and $a(\omega) = (\frac{\omega}{\Delta_0} - i\frac{\sqrt{\Delta_0^2-\omega^2}}{\Delta_0})$ and Φ is the diagonal matrix with diagonal elements $\{\phi_1, \phi_2\}$. Hence, the Andreev bound state energies are obtained as [39]

$$\omega_0^{\pm} = \pm\Delta_0\sqrt{\tau}\cos(\phi/2), \tag{7}$$

where $\phi = \phi_2 - \phi_1$ and $\tau = |t|^2$.

For energies $\omega > \Delta_0$, we calculate the total quasiparticle transmission probability ($\mathcal{T}^{i,j}$) from terminal i to terminal j ($i, j \in \{1, 2\}$ and $i \neq j$). We first consider an electronlike quasiparticle incident on the superconducting lead 1. It will give rise to a reflected electronlike and holelike quasiparticle within the same lead with amplitudes, say, r_{ee} and r_{he}, respectively, and transmitted electronlike and holelike quasiparticles in superconducting lead 2 with amplitudes, say, $t_{ee}^{2,1}$ and $t_{he}^{2,1}$, respectively. The BdG wave functions in different regions are given by

$$\Psi_{S1} = \frac{\exp\left[i\left(\frac{\mu+\sqrt{\omega^2-\Delta_0^2}}{\hbar v_F}\right)x\right]}{\sqrt{2\cosh(\theta)}}\begin{pmatrix} e^{\theta/2}e^{i\phi_1/2} \\ 0 \\ e^{-\theta/2}e^{-i\phi_1/2} \\ 0 \end{pmatrix} + \frac{r_{ee}\exp\left[-i\left(\frac{\mu+\sqrt{\omega^2-\Delta_0^2}}{\hbar v_F}\right)x\right]}{\sqrt{2\cosh(\theta)}}\begin{pmatrix} 0 \\ e^{\theta/2}e^{i\phi_1/2} \\ 0 \\ e^{-\theta/2}e^{-i\phi_1/2} \end{pmatrix}$$
$$+ \frac{r_{hh}\exp\left[i\left(\frac{\mu-\sqrt{\omega^2-\Delta_0^2}}{\hbar v_F}\right)x\right]}{\sqrt{2\cosh(\theta)}}\begin{pmatrix} e^{-\theta/2}e^{i\phi_1/2} \\ 0 \\ e^{\theta/2}e^{-i\phi_1/2} \\ 0 \end{pmatrix}, \tag{8}$$

$$\Psi_{S2} = \frac{t_{ee}^{2,1}\exp\left[i\left(\frac{\mu+\sqrt{\omega^2-\Delta_0^2}}{\hbar v_F}\right)x\right]}{\sqrt{2\cosh(\theta)}}\begin{pmatrix} e^{\theta/2}e^{i\phi_2/2} \\ 0 \\ e^{-\theta/2}e^{-i\phi_2/2} \\ 0 \end{pmatrix} + \frac{t_{he}^{2,1}\exp\left[-i\left(\frac{\mu-\sqrt{\omega^2-\Delta_0^2}}{\hbar v_F}\right)x\right]}{\sqrt{2\cosh(\theta)}}\begin{pmatrix} 0 \\ e^{-\theta/2}e^{i\phi_2/2} \\ 0 \\ e^{\theta/2}e^{-i\phi_2/2} \end{pmatrix}, \tag{9}$$

$$\Psi_{N(1,2)} = p_{(1,2)}\exp\left[i\left(\frac{\mu+\omega}{\hbar v_F}\right)x\right]\begin{pmatrix}1\\0\\0\\0\end{pmatrix} + q_{(1,2)}\exp\left[-i\left(\frac{\mu+\omega}{\hbar v_F}\right)x\right]\begin{pmatrix}0\\1\\0\\0\end{pmatrix} + r_{(1,2)}\exp\left[i\left(\frac{\mu-\omega}{\hbar v_F}\right)x\right]\begin{pmatrix}0\\0\\1\\0\end{pmatrix}$$
$$+ s_{(1,2)}\exp\left[-i\left(\frac{\mu-\omega}{\hbar v_F}\right)x\right]\begin{pmatrix}0\\0\\0\\1\end{pmatrix}, \tag{10}$$

where $\theta = \operatorname{arccosh}(\omega/\Delta_0)$. The subscripts $S(N)i$ denote the superconducting (normal) region in the ith ($i \in \{1, 2\}$) terminal. The coefficients p_i, q_i, r_i, and s_i denote the right-moving electronlike, left-moving electronlike, left-moving holelike, and right-moving holelike probability amplitudes for the quasiparticle wave functions within the normal region, in terminal i ($i \in \{1, 2\}$). Note that, in Fig. 1, if we divide the edge into left and right halves by drawing an imaginary line across the $x = 0$ point, then the left and right halves will be labeled as terminal 1 and terminal 2, respectively. By demanding continuity of the wave functions at the boundaries and assuming that the amplitudes of the incoming and the outgoing waves at $x = 0$ are related by the scattering matrices (4) and (6), we evaluate $\mathcal{T}_{e,e}^{2,1} = |t_{ee}^{2,1}|^2$ and $\mathcal{T}_{h,e}^{2,1} = |t_{he}^{2,1}|^2$. Similarly, for a holelike quasiparticle incident on the first superconducting lead, we calculate $\mathcal{T}_{e,h}^{2,1} = |t_{eh}^{2,1}|^2$ and $\mathcal{T}_{h,h}^{2,1} = |t_{hh}^{2,1}|^2$. Note that, for short junction limit $\mathcal{T}_e^{i,j} = \mathcal{T}_h^{i,j}$. The total quasiparticle transmission probability across the Josephson junction described by Eq. (3), $\mathcal{T}^{2,1}$, can be obtained as

$$\mathcal{T}^{2,1}(\omega,\tau,\phi) = \tau\left[\frac{2(\omega^2-\Delta_0^2)(\omega^2-|\omega_0^{\pm}|^2)}{\prod_{\omega_0}(\omega-\omega_0)^2}\right]\Theta\left(|\omega|^2-\Delta_0^2\right)$$
$$= 2\tau\left[\frac{\omega^2-\Delta_0^2}{\omega^2-|\omega_0^{\pm}|^2}\right]\Theta\left(|\omega|^2-\Delta_0^2\right). \tag{11}$$

The expression of bound state energy [Eq. (7)] and corresponding $\mathcal{T}^{2,1}$ given above are valid for the 1D Majorana-Josephson junction based on either (a) 1D Dirac fermions with proximitized s-wave superconductivity discussed above or for (b) 1D spinless electrons with quadratic dispersion and proximitized p-wave superconductivity [57,58].

However, the general form for $\mathcal{T}$ in the case of the 1D Josephson junction in the short junction limit can be expressed as

$$\mathcal{T}^{2,1}(\omega,\tau,\phi) = \tau\left[\frac{2\left(\omega^2-\Delta_0^2\right)\mathfrak{f}(\omega,\tau,\phi)}{(\omega^2-|\omega_0^{\pm}(\tau,\phi)|^2)^2}\right]\Theta\left(|\omega|^2-\Delta_0^2\right). \tag{12}$$

For the Majorana-Josephson junction, $\mathfrak{f}(\omega,\tau,\phi) = (\omega^2 - |\omega_0^{\pm}(\tau,\phi)|^2)$, which cancels with its square appearing in the denominator and hence leading to a ϕ dependence of $\mathcal{T}$ solely via the ϕ dependence of energy of the Andreev bound state ($\omega_0^{\pm}$) appearing in the denominator. Also, the τ dependence of $\mathcal{T}$ enters solely via $\omega_0(\tau,\phi)$ except for the expected overall multiplicative dependence on τ as shown in the right-hand side of Eqs. (11) and (12). In contrast, for the nontopological Josephson junction, $\mathfrak{f}(\omega,\tau,\phi) = (\omega^2 - \Delta_0^2\cos\phi - \tau\Delta_0^2\sin^2\phi/2)$ [4,5], which leads to a complicated

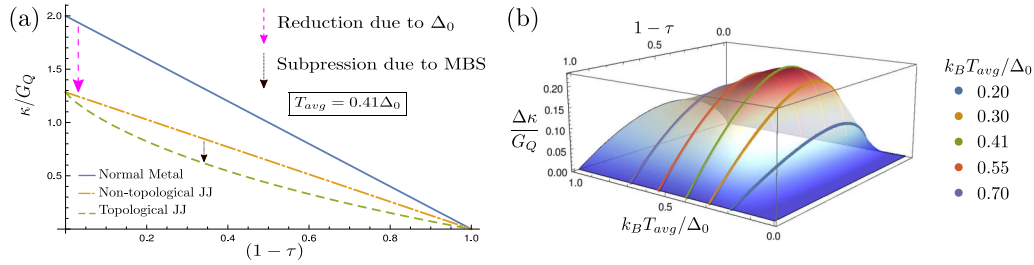

FIG. 2. (a) Plot of thermal conductance κ for $\phi = 0$ in units of G_Q as a function of τ for a normal junction (nonsuperconducting) and the corresponding nontopological and topological Josephson junctions. (b) Three-dimensional surface plot of the difference between the topological and nontopological cases in the (1-τ)-($k_BT_{\rm avg}/\Delta_0$) plane.

(ϕ, τ) dependence of $\mathcal{T}$. We will show the above discussed observations pave the way to the identification of a distinctive correlation between the electrical and thermal currents of a three-terminal Majorana-Josephson junction which carry signatures of isolated MESs.

B. Signatures of Majorana end state in two-terminal thermal conductance

We first discuss signatures of the Majorana-Josephson junction pertaining to its τ dependence in thermal conductance in the simplest case of $\phi = 0$. For a non-Majorana Josephson junction, $\mathcal{T}^{2,1}(\omega, \tau, \phi = 0) = 2\,\tau$ (see Appendix A), thus the thermal conductance of such a Josephson junction in the absence of phase bias is given by [using Eq. (2)] $\kappa = 2\,\tau[G_Q - \int_0^{\Delta_0} d\omega\,\omega\, df(\omega, T)/dT]_{T=T_{\rm avg}}$ where $G_Q = \pi^2 k_B^2 T/(3h)$ is the quantized thermal conductance of a single ballistic channel and the factor of 2 represents the doubling due to contributions from particle and hole channels. Hence it equals two times the normal-state thermal conductance suppressed up to the gap [4,5] [see Fig. 2(a)]. But for the Majorana-Josephson junction, $\mathcal{T}^{1,2}(\omega, \tau, \phi = 0) = 2\,\tau(1 - \alpha)$ where $\alpha = \Delta_0^2[(1-\tau)/(\omega^2 - \tau\Delta_0^2)]$, which implies an additional suppression proportional to α with respect to the nontopological Josephson junction. This contrast between the Majorana and the non-Majorana case stems from the fact that at zero phase bias ($\phi = 0$) the Andreev bound state energy stays pinned at $\omega_0^{\pm} = \pm\,\Delta_0$ and hence is independent of transmissivity (τ) of the junction for the non-Majorana case. On the contrary the bound state energy $|\omega_0^{\pm}| < \Delta_0$ for the Majorana case for $\phi = 0$ depends on τ. Hence this additional suppression of the thermal conductance of the Majorana-Josephson junction at $\phi = 0$ [see Fig. 2(b)] is a direct manifestation of MESs. Here we have assumed that each supercondcutor participating at the junction is a topological superconductor which hosts an end state that can either be Majorana or not Majorana. An example of a topological zero-energy end state which is not a Majorana was recently discussed by Marra and Nitta [50]. Hence a Josephson junction constructed from such a junction will also show suppression of thermal conductance. This is due to the fact that both the MESs and the nontrivial Andreev bound states, although being topologically inequivalent, have similar spectral signatures, i.e., with the decrease in transmissivity (τ) the Andreev bound state energies tend toward zero energy. This results in a decreasing density of states for the BdG quasiparticles thereby suppressing thermal conductance across the junction. However, a clear distinction can be made between topologically nontrivial Andreev type end states and the MESs, once we focus on a three-terminal Josephson junction, which is the next topic of discussion in this work.

Note that, for a junction between an odd number of 1D topological superconductors, each of which is hosting Majorana fermions at its end, a generic tunnel coupling at the junction will hybridize all the MESs leaving behind a single zero-energy MES at the junction. This is not true for the 1D topological superconductors discussed in Ref. [50], and this distinction forms the basis for exploring a three-terminal Josephson junction. In this regard we would like to point out that distinguishing signatures of MESs has been a topic of intense research [59–63], though the focus has mostly been on the nanowire realization of MESs rather than on the case of helical edge states. Now we start focusing on quantifying the correlation between κ and the Josephson current discussed above. From (2) and (12) we note that the thermal conductance of a topological Josephson junction can be expressed as

$$\kappa = \sigma^N \left[\frac{2}{e^2\beta(T)}\int_{\Delta_0}^{\infty} d\omega\,\omega \frac{(\omega^2 - \Delta_0^2)}{[\omega^2 - |\omega_0^{\pm}(\tau,\phi)|^2]}\frac{df(\omega,T)}{dT}\right]_{T=T_{\rm avg}}, \tag{13}$$

where $\sigma^N = (e^2\tau/h)\beta(T)$ is Landauer-Buttiker conductance [64,65] at finite temperature where $\beta(T) = \int_{-\infty}^{\infty}(-\partial f/\partial\omega)d\omega = (4k_BT)^{-1}\int_{-\infty}^{\infty}[\cosh(\frac{\omega}{2k_BT})]^{-2}d\omega$ is the thermal broadening factor. We also note that the Josephson current (I^J) at temperature T is given by [47]

$$I^J = -\frac{2e}{\hbar}\frac{\partial|\omega_0^{\pm}|}{\partial\phi}\tanh\left(\frac{|\omega_0^{\pm}|}{2k_BT}\right). \tag{14}$$

Now it is straightforward to note that the Josephson current can be related to the corresponding thermal conductance of the topological Josephson junction via the relation (see Appendix B)

$$\partial_\phi\kappa = \sigma^N I^J\left[\frac{-h|\omega_0^{\pm}|}{\pi e^3}\left\{\frac{1}{\beta(T)}\coth\left(\frac{|\omega_0^{\pm}|}{2k_BT}\right)\right\}\int_{\Delta_0}^{\infty} d\omega\,\omega\frac{\omega^2 - \Delta_0^2}{(\omega^2 - |\omega_0^{\pm}|^2)^2}\frac{df(\omega,T)}{dT}\right]_{T=T_{\rm avg}}, \tag{15}$$

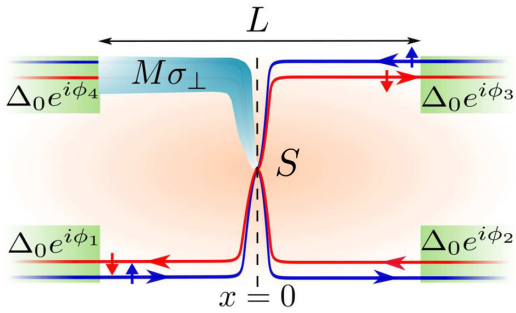

FIG. 3. Pictorial representation of an effective three-terminal Josephson junction depicted on a helical edge state of quantum spin Hall bar geometry where S represents scattering at $x = 0$ due to the quantum point contact. $M\sigma_\perp$ represents a local magnetic field perpendicular to the spin-quantization axis of the helical edge state.

which directly exploits the fact that the ϕ dependence in both I^J and κ stem from the ϕ dependence of ω_0. We show next that the three-terminal thermal conductance also follows the same relation between $\partial_{\phi_{kl}}\kappa_{i,j}$ and corresponding $\sigma^N_{i,j}$, $I^J_{i,j}$ $(i, j = 1, 2, 3)$ owing to the presence of topologically protected MESs at the trijunction. This fact leads to our central result presented in Eqs. (31) and (32).

IV. THREE-TERMINAL MAJORANA-JOSEPHSON JUNCTION IN HELICAL EDGE STATE

A. The model

We consider a standard Hall bar type geometry (see Fig. 3) hosting a quantum spin Hall state comprising an upper and a lower helical edge state with opposite helicity, which are extended from $x = -\infty$ to $x = +\infty$, and additionally a quantum point contact is considered at the $x = 0$, which enables local coherent scattering between the upper and the lower edge. The BdG Hamiltonian describing the edges is given by

$$\begin{aligned}\mathcal{H}_\eta &= H_{\text{edge}} + H_{\text{Zeeman}} \\ &= \{(\eta v_F \hat{p}_x\sigma_z - \mu)\tau_z + \Delta(x)(\cos\phi_r\tau_x - \sin\phi_r\tau_y)\} \\ &\quad + \{(\eta-1)/2\}M(x)\sigma_\perp, \end{aligned} \tag{16}$$

where σ and τ have their usual meaning as defined earlier, η defines the helicity of the edge state, $\eta = 1$ for the lower edge and $\eta = -1$ for the upper edge, and we have assumed the proximity-induced s-wave superconductivity to be present on the edges in the interval $(x = \pm\infty, \pm L/2]$ [i.e., $\Delta(x) \neq 0$] where each of the superconductors may have independent phase for their respective order parameters given by $\Delta_0 e^{i\phi_r}$ where $[r \in \{1, 2\}]$ are labels for superconducting patches on the lower edge corresponding to $(x = \mp\infty, \mp L/2]$, respectively, and $[r \in \{3, 4\}]$ stands for the upper edge corresponding to $(x = \pm\infty, \pm L/2]$, respectively. A local Zeeman field is assumed to be present at the upper edge such that $M(x) = M_0\Theta(x + L/2)\Theta(-x)$ and $M_0 \to \infty$, which cuts off the superconducting contact at $r = 4$ hence reducing it to a three-terminal Josephson junction.

We also impose a scattering matrix, S, at $x = 0$, which represents the quantum point contact and its elements are such that $|(S)_{i,j}| = |(S)_{j,i}|$ $(i, j = 1, 2, 3)$ so that the scattering matrix for electrons takes the form

$$S^e = \begin{pmatrix} r_{11} & t_{12} & t_{13} \\ t_{21} & r_{22} & t_{23} \\ t_{31} & t_{32} & r_{33} \end{pmatrix}. \tag{17}$$

Here r_{ii} represents the amplitude of back-reflection within the terminal i and t_{ji} represents the amplitude of transmission from terminal i to terminal j. The derivation of such scattering matrix within a tunneling Hamiltonian approach is provided in Appendix C.

For energy $\omega < \Delta_0$ (measured with respect to μ), the condition for the formation of Andreev bound state is given by

$$\det[\mathbb{I} - a^2(\omega)S^e e^{i\Phi}S^h e^{-i\Phi}] = 0, \tag{18}$$

where $a(\omega) = (\frac{\omega}{\Delta_0} - i\frac{\sqrt{\Delta_0^2-\omega^2}}{\Delta_0})$, Φ is the diagonal matrix with diagonal elements $\{\phi_1, \phi_2, \phi_3\}$, and S^h is the scattering matrix for hole and is given by

$$S^h = \begin{pmatrix} -r^*_{11} & t^*_{12} & -t^*_{13} \\ t^*_{21} & -r^*_{22} & t^*_{23} \\ -t^*_{31} & t^*_{32} & -r^*_{33} \end{pmatrix}, \tag{19}$$

which can be obtained by imposing the particle-hole symmetry (for details see Appendix C). After some algebraic manipulations we obtain the bound state energies (ω_0) given by

$$\omega_0^0 = 0, \tag{20}$$

$$\omega_0^\pm = \pm\Delta_0\sqrt{\tau_{12}\cos^2\frac{\phi_{12}}{2} + \tau_{13}\sin^2\frac{\phi_{13}}{2} + \tau_{23}\cos^2\frac{\phi_{23}}{2}}, \tag{21}$$

where $\phi_{ij} = \phi_j - \phi_i$ [66]. Insight into the form of subgap bound state solution can be obtained by considering an effective Majorana Hamiltonian where each superconducting terminal $(i = 1, 2, 3)$ is expected to contribute one Majorana each to the junction except the fourth terminal where the Majorana has been pushed away owing to the Zeeman gap. The effective Majorana Hamiltonian then takes the form [39,67,68]

$$H = \frac{i}{2}\sum_{1\leqslant a\leqslant b\leqslant 4}\xi_{ab}\gamma_a\gamma_b, \tag{22}$$

where $\xi_{ab} = \frac{\Delta_0}{2}\sqrt{\tau_{ab}}\cos(\frac{\phi_{ab}}{2} - \frac{\chi_{ab}}{2})$ and γ_a is the Majorana zero mode operator corresponding to terminal $a = 1, 2, 3, 4$. We consider $\chi_{ii} = \chi_{13} = \chi_{24} = \pi$, which incorporates the excess Berry phase due to spin-flip scattering at the quantum point contact. To mimic the three-terminal situation described by Eq. (16) we take $\tau_{i4} = \tau_{4i} = 0$ for $i \neq 4$ and hence $\xi_{14} = \xi_{24} = \xi_{34} = 0$. This Majorana Hamiltonian readily provides two zero-energy eigenvalues and the other two eigenvalues being identical to $\omega_0^\pm$ given above. Note that three of these eigenstates correspond to hybridized γ_1, γ_2, and γ_3 resulting in an MES that stays pinned to zero energy $(\epsilon = 0)$ and a pair of Andreev bound states at energy $\epsilon_\pm = \omega_0^\pm$ while the fourth zero-energy state corresponds to the MES, which stays away from the junction due to the Zeeman gap.

B. Three-terminal thermal conductance

Returning back to the Hamiltonian (16), for energies $\omega > \Delta_0$, we calculate the total quasiparticle transmission probability ($\mathcal{T}^{j,i}$) from terminal i to terminal j. We first consider an electronlike quasiparticle incident on the superconducting lead 1. It will give rise to a reflected electronlike and holelike quasiparticle within the same lead with amplitudes, say, r_{ee} and r_{he}, respectively, and transmitted electronlike and holelike quasiparticles in superconducting nth lead with amplitudes, say, $t_{ee}^{n,1}$ and $t_{he}^{n,1}$, respectively.

The wave functions for the three-lead problem can be written as

$$\Psi_{S1} = \frac{\exp\left[i\left(\frac{\mu+\sqrt{\omega^2-\Delta_0^2}}{\hbar v_F}\right)x\right]}{\sqrt{2\cosh(\theta)}}\begin{pmatrix} e^{\theta/2}e^{i\phi_1/2} \\ 0 \\ e^{-\theta/2}e^{-i\phi_1/2} \\ 0 \end{pmatrix} + \frac{r_{ee}\exp\left[-i\left(\frac{\mu+\sqrt{\omega^2-\Delta_0^2}}{\hbar v_F}\right)x\right]}{\sqrt{2\cosh(\theta)}}\begin{pmatrix} 0 \\ e^{\theta/2}e^{i\phi_1/2} \\ 0 \\ e^{-\theta/2}e^{-i\phi_1/2} \end{pmatrix}$$
$$+ \frac{r_{hh}\exp\left[i\left(\frac{\mu-\sqrt{\omega^2-\Delta_0^2}}{\hbar v_F}\right)x\right]}{\sqrt{2\cosh(\theta)}}\begin{pmatrix} e^{-\theta/2}e^{i\phi_1/2} \\ 0 \\ e^{\theta/2}e^{-i\phi_1/2} \\ 0 \end{pmatrix}, \tag{23}$$

$$\Psi_{S2} = \frac{t_{ee}^{2,1}\exp\left[i\left(\frac{\mu+\sqrt{\omega^2-\Delta_0^2}}{\hbar v_F}\right)x\right]}{\sqrt{2\cosh(\theta)}}\begin{pmatrix} e^{\theta/2}e^{i\phi_2/2} \\ 0 \\ e^{-\theta/2}e^{-i\phi_2/2} \\ 0 \end{pmatrix} + \frac{t_{he}^{2,1}\exp\left[-i\left(\frac{\mu-\sqrt{\omega^2-\Delta_0^2}}{\hbar v_F}\right)x\right]}{\sqrt{2\cosh(\theta)}}\begin{pmatrix} 0 \\ e^{-\theta/2}e^{i\phi_2/2} \\ 0 \\ e^{\theta/2}e^{-i\phi_2/2} \end{pmatrix}, \tag{24}$$

$$\Psi_{S3} = \frac{t_{ee}^{3,1}\exp\left[i\left(\frac{\mu+\sqrt{\omega^2-\Delta_0^2}}{\hbar v_F}\right)x\right]}{\sqrt{2\cosh(\theta)}}\begin{pmatrix} 0 \\ e^{\theta/2}e^{i\phi_3/2} \\ 0 \\ e^{-\theta/2}e^{-i\phi_3/2} \end{pmatrix} + \frac{t_{he}^{3,1}\exp\left[-i\left(\frac{\mu-\sqrt{\omega^2-\Delta_0^2}}{\hbar v_F}\right)x\right]}{\sqrt{2\cosh(\theta)}}\begin{pmatrix} e^{-\theta/2}e^{i\phi_3/2} \\ 0 \\ e^{\theta/2}e^{-i\phi_3/2} \\ 0 \end{pmatrix}, \tag{25}$$

$$\Psi_{N(1,2)} = p_{(1,2)}\exp\left[i\left(\frac{\mu+\omega}{\hbar v_F}\right)x\right]\begin{pmatrix}1\\0\\0\\0\end{pmatrix} + q_{(1,2)}\exp\left[-i\left(\frac{\mu+\omega}{\hbar v_F}\right)x\right]\begin{pmatrix}0\\1\\0\\0\end{pmatrix} + r_{(1,2)}\exp\left[i\left(\frac{\mu-\omega}{\hbar v_F}\right)x\right]\begin{pmatrix}0\\0\\1\\0\end{pmatrix}$$
$$+ s_{(1,2)}\exp\left[-i\left(\frac{\mu-\omega}{\hbar v_F}\right)x\right]\begin{pmatrix}0\\0\\0\\1\end{pmatrix}, \tag{26}$$

$$\Psi_{N3} = p_3\exp\left[i\left(\frac{\mu+\omega}{\hbar v_F}\right)x\right]\begin{pmatrix}0\\1\\0\\0\end{pmatrix} + q_3\exp\left[-i\left(\frac{\mu+\omega}{\hbar v_F}\right)x\right]\begin{pmatrix}1\\0\\0\\0\end{pmatrix} + r_3\exp\left[i\left(\frac{\mu-\omega}{\hbar v_F}\right)x\right]\begin{pmatrix}0\\0\\0\\1\end{pmatrix}$$
$$+ s_3\exp\left[-i\left(\frac{\mu-\omega}{\hbar v_F}\right)x\right]\begin{pmatrix}0\\0\\1\\0\end{pmatrix}, \tag{27}$$

where $\theta = \operatorname{arccosh}(\omega/\Delta_0)$. The subscripts $S(N)i$ denote the superconducting (normal) region in the ith ($i \in \{1, 2, 3\}$) terminal. The coefficients p_i, q_i, r_i, and s_i denote the probability amplitude for the right-moving electronlike, left-moving electronlike, left-moving holelike, and right-moving holelike quasiparticle wave functions within the normal region, in terminal i ($i \in \{1, 2, 3\}$).

By demanding continuity of the wave functions at the boundaries and assuming that the amplitudes of the incoming and the outgoing waves at $x = 0$ are related by the scattering matrices (17) and (19), we evaluate $\mathcal{T}_e^{2,1} = |t_{ee}^{2,1}|^2 + |t_{he}^{2,1}|^2$ and $\mathcal{T}_e^{3,1} = |t_{ee}^{3,1}|^2 + |t_{he}^{3,1}|^2$. Similarly, for a holelike quasiparticle incident on the first superconducting lead, we calculate $\mathcal{T}_h^{2,1} = |t_{hh}^{2,1}|^2 + |t_{eh}^{2,1}|^2$ and $\mathcal{T}_h^{3,1} = |t_{hh}^{3,1}|^2 + |t_{eh}^{3,1}|^2$. The total quasiparticle transmission probability from terminal 1 to terminal 2 and terminal 3 across the Josephson junction described by Eq. (16), $\mathcal{T}^{2,1}$ and $\mathcal{T}^{3,1}$, can be obtained, as discussed in Sec. II:

$$\mathcal{T}^{2,1} = \tau_{12}\left[\frac{2\,\omega^2\left(\omega^2-\Delta_0^2\right)\left(\omega^2-|\omega_0^{\pm}|^2\right)}{\prod_{\omega_0}(\omega-\omega_0)^2}\right]\Theta\left(|\omega|^2-\Delta_0^2\right)$$
$$= 2\tau_{12}\left[\frac{\left(\omega^2-\Delta_0^2\right)}{\omega^2-|\omega_0^{\pm}|^2}\right]\Theta\left(|\omega|^2-\Delta_0^2\right), \tag{28}$$

$$\mathcal{T}^{3,1} = \tau_{13}\left[\frac{2\,\omega^2\big(\omega^2-\Delta_0^2\big)\big(\omega^2-|\omega_0^{\pm}|^2\big)}{\prod_{\omega_0}(\omega-\omega_0)^2}\right]\Theta\big(|\omega|^2-\Delta_0^2\big)$$
$$= 2\tau_{13}\left[\frac{\big(\omega^2-\Delta_0^2\big)}{\omega^2-|\omega_0^{\pm}|^2}\right]\Theta\big(|\omega|^2-\Delta_0^2\big), \tag{29}$$

where $\omega_0^{\pm}$ is given by Eq. (21). With the same spirit we can calculate other $\mathcal{T}^{i,j}$. In general, the total quasiparticle transmission probability from terminal j to terminal i is given by

$$\mathcal{T}^{i,j}(\omega,\tau_{ij},\phi_{ij}) = \tau_{ij}\left[\frac{2\big(\omega^2-\Delta_0^2\big)\,\mathfrak{f}(\omega,\tau_{ij},\phi_{ij})}{\prod_{\omega_0}\left[\omega-\omega_0(\tau_{ij},\phi_{ij})\right]^2}\right]$$
$$\times\,\Theta\big(|\omega|^2-\Delta_0^2\big), \tag{30}$$

where $[i,j\in\{1,2,3\}, j>i]$ and $\mathfrak{f}=\omega^2(\omega^2-|\omega_0^{\pm}|^2)$.

C. Signatures of Majorana end state in three-terminal thermal conductance

The resulting expression of $\mathcal{T}^{n,m}$ in Eq. (30) has a perfect congruence with the two-terminal case (see Eq. (12)] due to cancellation of ω^2 in the numerator with $[\omega-\omega_0(\tau_{ij},\phi_{ij})]^2_{\omega_0=\omega_0^0}$ in the denominator owing to the MES at $\omega_0=\omega_0^0=0$. This similarity immediately validates Eqs. (13) and (15) for the three-terminal case also, where $\kappa\to\kappa_{i,j}$, $\phi\to\phi_{ij}$, $\sigma^N\to\sigma^N_{i,j}$, and $I^J\to I^J_{i,j}$ and hence leads to the following relations given by

$$\frac{\kappa_{i,j}}{\kappa_{k,l}} = \frac{\sigma^N_{i,j}}{\sigma^N_{k,l}}, \tag{31}$$

$$\frac{\partial_{\phi_{kl}}\kappa_{i,j}/I^J_{k,l}}{\partial_{\phi_{pq}}\kappa_{m,n}/I^J_{p,q}} = \frac{\sigma^N_{i,j}}{\sigma^N_{m,n}}. \tag{32}$$

Here $i,j,k,l\in\{1,2,3\}$ and $j\neq i, l\neq k$. The above two equations constitute the central result of this paper. It is remarkable that the ratios of normal-state multiterminal conductance ($\sigma^N_{i,j}$) equates the ratio of corresponding multiterminal thermal conductance ($\kappa_{i,j}$) for a topological Josephson junction, though individually they are complicated functions of $T_{\rm avg}$, ω_0, and Δ_0. $\sigma^N_{i,j}$ being independent of $\phi_{i,j}$, hence the ratios of $\kappa_{i,j}$ are also independent of $\phi_{i,j}$ though individually they are periodic functions of $\phi_{i,j}$. This results from the special $\tau_{i,j}$ dependence of $\mathcal{T}^{i,j}$ which is solely via $\tau_{i,j}$ dependence of $\omega_0(\tau_{i,j},\phi_{i,j})$ except for an overall multiplicative dependence [see Eq. (30)]. It is also remarkable that the ratio of Josephson current and the phase derivative of thermal conductance [see Eq. (32)] leads to ratios which are independent of $T_{\rm avg}$, ω_0, and Δ_0 and the phase bias though both phase-derivative of thermal conductance and the Josephson current have strong dependence on these parameters.

We reemphasize that Eqs. (31) and (32) results form the fact that expression for $\mathcal{T}^{n,m}$ for the three-terminal case has a perfect congruence with the corresponding expression for the two-terminal case. This congruence results from the fact that in both cases the subgap state in the short junction limit corresponds to a pair of hybridized Majorana fermions whose energy has an identical dependence on τ and ϕ. The three-terminal case has an extra zero-energy state (the third Majorana) which is insensitive to τ and ϕ hence does not disturb this congruence. Hence this congruence and the resulting Eqs. (31) and (32) can be taken as a signature of Majorana fermions. For a finite superconductor, it is expected that the MES at the junction and their corresponding partner MES on the other ends of the superconducting wires will have a finite overlap and this fact might disturb the validity of our results. But one needs to take into consideration the fact that the overlap between all the MESs at the junction is expected to be much stronger than the overlap between partner MESs living on the other ends of the superconducting wire. If the energy scale associated with the overlap of partner MESs on the two ends of the superconductor is of the same order as the $k_BT_{\rm avg}$, then such effects will be of little consequence and we expect our results to stay valid. The other important question is, does the validity of Eqs. (31) and (32) necessarily imply the presence of Majorana fermions or can they be mimicked by other topological bound states appearing at the ends of the superconductor and pinned zero energy which we call the "Andreev end state," for example, of the type discussed in Ref. [50] as mentioned earlier? We have shown in Sec. IV E via numerical analysis that, when such end states are tunnel coupled at a three-terminal junction via a generic tunnel coupling, it always results in full hybridization of these zero modes leaving behind no zero-energy state unlike MESs and hence spoiling the congruence in the expression for $\mathcal{T}^{n,m}$ between the two-terminal and three-terminal setup.

D. Short junction limit vs finite length junctions for three-terminal Majorana-Josephson junction

Equations (31) and (32) are derived in the short junctions ($L\ll\xi$), hence it is important to study how violation of these relations sets in as we move to the long junction limit. For quantifying the violation we study the three-terminal Josephson junction given in Fig. 3 based on helical edge states with finite junction length L for the normal region on each arm of the Josephson junction. We consider a scattering matrix (for electrons) as provided in Eq. (17) with the scattering matrix elements given by

$$r_{11} = r_{22} = -\lambda, \tag{33}$$

$$r_{33} = 1-2\lambda, \tag{34}$$

$$t_{12} = t_{21} = 1-\lambda, \tag{35}$$

$$t_{13} = t_{31} = -i\sqrt{2\lambda(1-\lambda)} = t_{23} = t_{32}, \tag{36}$$

where $0\leqslant\lambda\leqslant 1$. Note that this scattering matrix is symmetric between terminal 1 and terminal 2. With the scattering matrix discussed above, we have calculated the transmission probabilities $\mathcal{T}^{i,j}$ following the discussed in Sec. IV A and hence calculated $\kappa_{i,j}$, which has been plotted in Fig. 4. For finite length junctions there are two contributions (I_1 and I_2) to the Josephson current as discussed in Appendix B and it is I_2 which will be primarily responsible for the violation of Eq. (32). To account for both the contributions we shall use the Matsubara sum [69] such that the Josephson current is

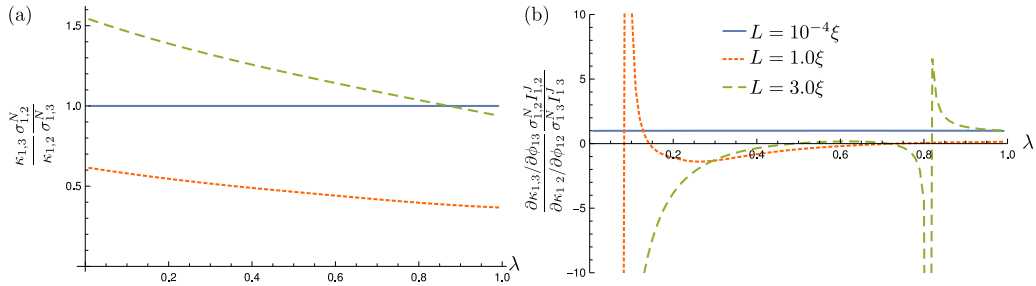

FIG. 4. The ratios (a) $(\kappa_{1,3}\sigma^N_{1,2})/(\kappa_{1,2}\sigma^N_{1,3})$ and (b) $[(\partial_{\phi_{13}}\kappa_{1,3})\sigma^N_{1,2}I^J_{1,2}]/[(\partial_{\phi_{12}}\kappa_{1,2})\sigma^N_{1,3}I^J_{1,3}]$ are plotted as a function of scattering matrix parameter $0 \leqslant \lambda \leqslant 1$ for different values of junction length L all for quantum point contact. Here $\xi = \hbar v_f/\Delta_0$ is the superconducting coherence length. Here we have assumed $\phi_{12} = 0.880\,850\pi$ and $\phi_{13} = 0.332\,947\pi$. For short junction limit these ratios are independent of scattering matrix parameters and phase differences as expected from our predictions but start drifting away form unity as we move to finite length junction limit. The average temperature is assumed to be $k_B T_{\text{avg}} = 0.5\Delta_0$.

given by

$$I^J_{i,j} = -\frac{2e}{\hbar} 2k_B T \frac{\partial}{\partial \phi_{ij}} \sum_{n=0}^{\infty} \ln \det[\mathbb{I} - a^2(i\omega_n) S^e e^{i\Phi} S^h e^{-i\Phi}], \tag{37}$$

where $a(\omega) = (\frac{\omega}{\Delta_0} - i\frac{\sqrt{\Delta_0^2-\omega^2}}{\Delta_0})$ and $\omega_n = (2n+1)\pi k_B T$ are the Matsubara frequencies. We have used Eq. (37) to produce the plot as shown in Fig. 4(b). We have evaluated the ratios $(\kappa_{1,3}\sigma^N_{1,2})/(\kappa_{1,2}\sigma^N_{1,3})$ [Fig. 4(a)] and $[(\partial_{\phi_{13}}\kappa_{1,3})\sigma^N_{1,2}I^J_{1,2}]/[(\partial_{\phi_{12}}\kappa_{1,2})\sigma^N_{1,3}I^J_{1,3}]$ [Fig. 4(b)] numerically with $\phi_{12} = 0.880\,850\pi$ and $\phi_{13} = 0.332\,947\pi$ for different values of junction length L as a function of scattering matrix parameter λ. It is clear from the plot that once we deviate from the limit of $L \ll \xi$, we get large deviations from the predictions of Eqs. (31) and (32).

E. Possibility of fake signatures of Majorana by other topological end state

In this section we will discuss a three-terminal Josephson junction comprising three 1D topological supercondcutors, each of which is described by a Hamiltonian given in Ref. [50] where the Hamiltonian hosts one trivial phase and two distinct topological phases of which one of the topological phases corresponds to the presence of a MES and the other topological phase corresponds to the presence of a zero-energy Andreev

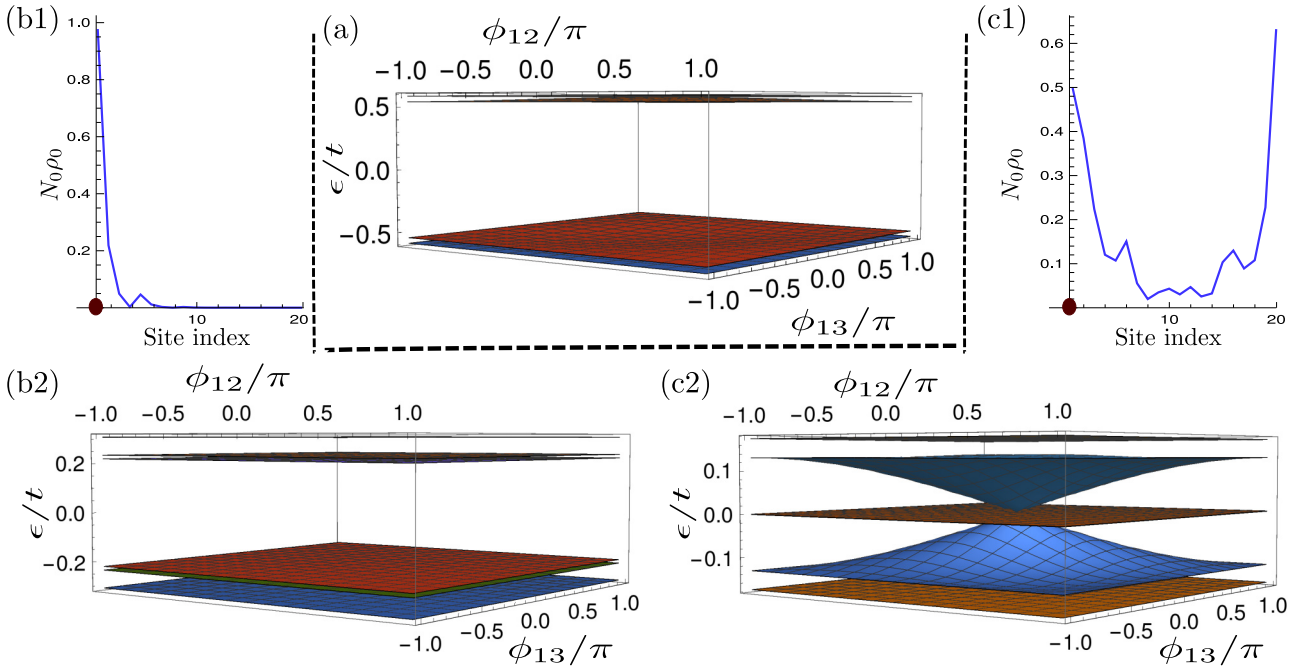

FIG. 5. Local probability density (ρ_0) (up to some normalization N_0) for an isolated arm of the trijunction is plotted in (b1) and (c1) for the case when the superconductor is hosting Andreev end state and MES, respectively. For both the cases a system comprising 20 sites is considered. The brown dots in (b1) and (c1) indicate the last site where the interwire tunneling is switched on while forming the junction. Subgap energy spectrum of the Josephson trijunction of the 1D system in its trivial phase, phase hosting Andreev end state, and MES are depicted in (a), (b2), and (c2), respectively. The tunneling strength at the junction is taken to be $0.6t$.

end state. The lattice Hamiltonian discussed above is given by

$$\mathcal{H} = \frac{1}{2}\sum_n \Psi_n^\dagger \cdot \begin{bmatrix} -\mu\sigma_0 + \vec{b}_n\cdot\vec{\sigma} & \Delta i\sigma_y \\ -(\Delta i\sigma_y)^* & \mu\sigma_0 - (\vec{b}_n\cdot\vec{\sigma})^* \end{bmatrix}\cdot\Psi_n - \frac{1}{2}\sum_n \Psi_n^\dagger \cdot \begin{bmatrix} t\sigma_0 - \lambda i\sigma_y & 0 \\ 0 & -(t\sigma_0 - \lambda i\sigma_y) \end{bmatrix}\cdot\Psi_{n+1} + \text{H.c.}, \tag{38}$$

where $\Psi_n^\dagger = [c_{n,\uparrow}^\dagger, c_{n,\downarrow}^\dagger, c_{n,\uparrow}, c_{n,\downarrow}]$ is the Nambu spinor, n is the site index of the 1D lattice, λ is the intrinsic spin-orbit coupling, t is the hopping parameter, and $\vec{b}_n\cdot\vec{\sigma} = b\sigma_z + \delta b\,\sin(n\theta+\chi)\sigma_x + \delta b\,\cos(n\theta+\chi)\sigma_z$ is the total Zeeman field at each site. We consider three copies of the above Hamiltonian to form a three-terminal junction where $\Delta = \Delta_0 e^{i\phi_r}$ and ϕ_r is the superconducting phase in lead r ($r = 1, 2, 3$). A tunneling proportional to $t\sigma_0$ is switched on among the leads. We have taken the parameters t, θ, μ, and Δ_0 to be the same as that provided in Ref. [50], i.e., $t = 1$, $\theta = \pi/2$, $\mu = -2t\cos(\theta/2)$, $\Delta_0 = \lambda = t/2$. With these parameter values we perform an exact diagonalization of junction comprising three arms, each of which has 20 lattice sites and the results of our analysis are plotted in Fig. 5. By setting $b = \delta b = 0$ we obtain the trivial phase; setting $\delta b = 1.5t$, $b = 2.5t$ ($\chi \approx 1.205\pi$ or $\approx 1.295\pi$) we get nontrivial Andreev end states while by setting $\delta b = 1.5t$, $b = 0.25t$ ($\chi = 0$) we obtain the state hosting MES. Figure 5(b1) shows the appearance of Andreev end states while Fig. 5(c1) shows the appearance of MES obtained from diagonalization of a Hamiltonian for an isolated arm of the trijunction of 20 lattice sites. We note from Fig. 5(c2) that the subgap spectrum for the topological Josephson trijunction hosting MES, the zero-energy state survives through the parameter regime considered in the plot while from Fig. 5(b2) we see that the Andreev end states completely hybridize and move away from the zero energy. This fact essentially leads us to the conclusion that topological end states of 1D superconductors which are distinct from MES will not lead to the results in Eqs. (31) and (32) in the short junction limit.

F. Topological vs nontopological three-terminal Josephson junction in short junction limit

Now we will demonstrate that the three-terminal Josephson junction of the 1D superconductor in nontopological phase shows large deviation from the results of Eqs. (31) and (32). To demonstrate this fact with an example, we consider a Josephson junction based on 1D electrons with quadratic dispersion and proximity-induced s-wave superconductivity. The superconducting leads of such a junction can be described by using the BdG Hamiltonian given below [57,70]:

$$\mathcal{H} = \left(-\frac{\hbar^2}{2m}\frac{\partial^2}{\partial x^2} - \mu\right)\tau_z + \Delta(x)[\cos\phi_i\tau_x - \sin\phi_i\tau_y], \tag{39}$$

where τ_n are the Pauli matrices acting on particle-hole basis; $\Delta(x) = \Delta_0\Theta(x - L)$ and ϕ_i is the superconducting phase of the ith superconducting lead. The system comprises three copies of the Hamiltonian given above which form the three superconducting leads and they extend from infinity to a distance L from the center of the junction and hence the junction

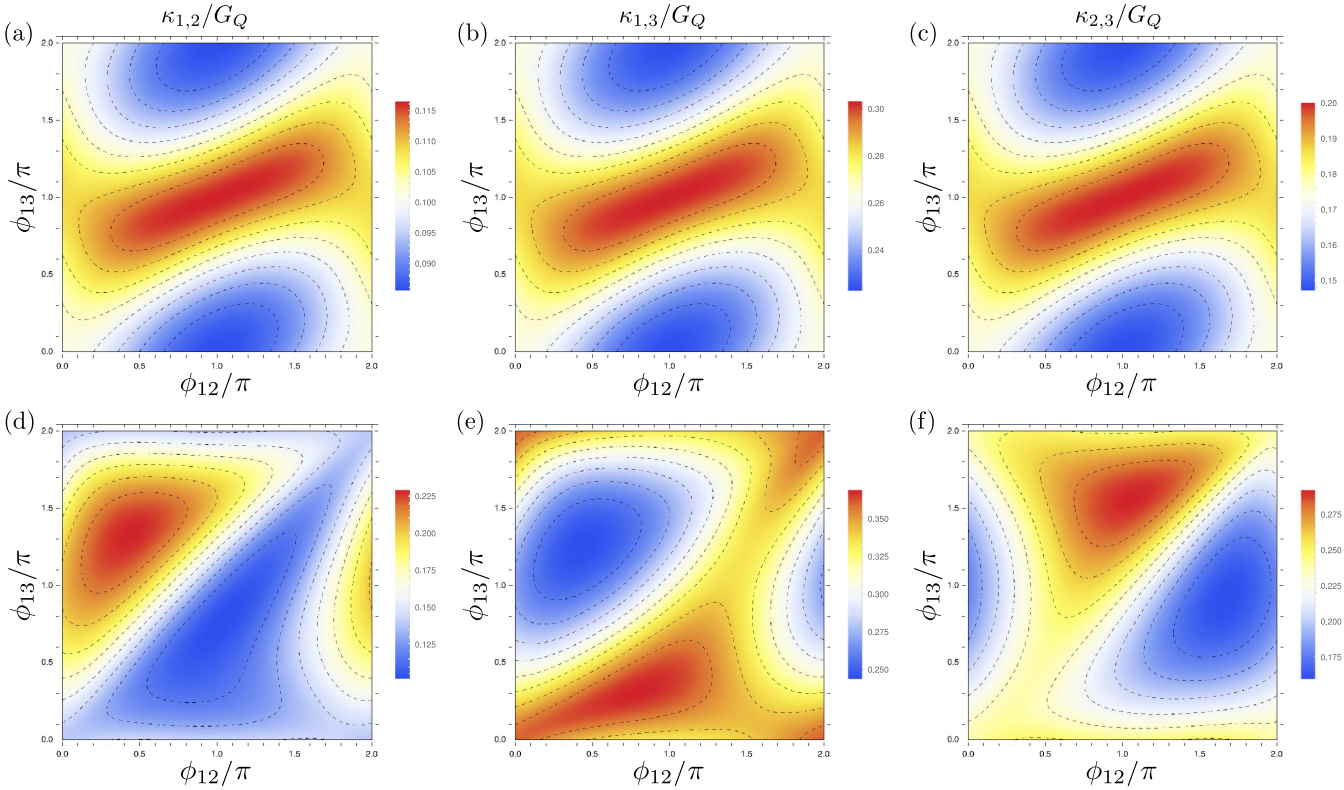

FIG. 6. Thermal conductances of a Josephson trijunction in the presence of zero-energy MES (a) $\kappa_{1,2}$, (b) $\kappa_{1,3}$, (c) $\kappa_{2,3}$, and in the absence of zero energy (d) $\kappa_{1,2}$, (e) $\kappa_{1,3}$, (f) $\kappa_{2,3}$ for the scattering matrix given in Eq. (40). Here the average temperature is assumed to be $k_BT = 0.5_i\Delta_0$.

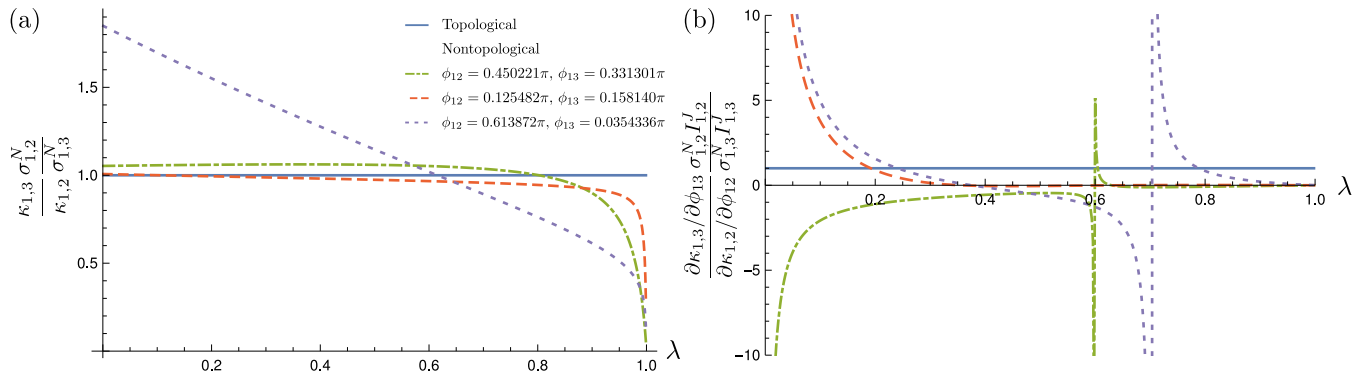

FIG. 7. The ratio $(\kappa_{1,3}\sigma^N_{1,2})/(\kappa_{1,2}\sigma^N_{1,3})$ plotted in (a) and $[(\partial_{\phi_{13}}\kappa_{1,3})\sigma^N_{1,2}I^J_{1,2}]/[(\partial_{\phi_{12}}\kappa_{1,2})\sigma^N_{1,3}I^J_{1,3}]$ plotted in (b), as a function of scattering matrix parameter $0 \leqslant \lambda \leqslant 1$ for different values of the independent phase differences ϕ_{12} and ϕ_{13}. For the topological case this ratio is independent of scattering matrix parameter(s) as well as phase differences and is pinned to unity as expected from our prediction unlike the nontopological case. Here the average temperature is assumed to be $k_B T_{\text{avg}} = 0.5\Delta_0$.

itself comprises three normal regions of length L on each arm. These three arms are then stitched together using a unitary scattering matrix given below to form the junction. Note that we also consider the superconductors to be highly doped and the scattering matrix (for electrons) at the junction to be symmetric and it is given by [71]

$$S^e = \begin{pmatrix} 0.496\,333 - 0.307\,063i & 0.292\,369 + 0.312\,308i & -0.324\,052 - 0.609\,377i \\ 0.292\,369 + 0.312\,308i & 0.588\,738 + 0.394\,712i & 0.008\,877\,01 + 0.560\,799i \\ -0.324\,052 - 0.609\,377i & 0.008\,877\,01 + 0.560\,799i & 0.446\,798 + 0.097\,199\,4i \end{pmatrix} \tag{40}$$

$(S^h = S^{e*})$ at the junction and we calculate the transmission probabilities and hence the thermal conductances $\kappa_{i,j}$ as discussed in Sec. IV B. We perform all these calculations numerically as the analytic expressions for the $\mathcal{T}^{n,m}$ in this case are cumbersome unlike the topological case discussed above. Using the scattering matrix in Eq. (40), we calculate the $\mathcal{T}^{i,j}$ and the corresponding thermal conductances $\kappa_{i,j}$. The thermal conductances $\kappa_{i,j}$ for the Majorana-Josephson junction discussed in the previous section and the present nontopological case are plotted together in Fig. 6. As can be clearly seen, in the case of a nontopological Josephson trijunction, apart from the overall suppression due to $\tau_{i,j}$, thermal conductances $\kappa_{i,j}$, in general, have a very different pattern in the parameter space of ϕ_{12} and ϕ_{13} (lower row of Fig. 6) whereas the exact same pattern (apart from overall suppression) of thermal conductances, in the case of a Majorana-Josephson trijunction (upper row of Fig. 6) arises. Now to quantify the deviation from the prediction of Eqs. (31) and (32) which is induced via the variation of the pattern mentioned above, we plot the ratio $(\kappa_{1,3}\sigma^N_{1,2})/(\kappa_{1,2}\sigma^N_{1,3})$ and $[(\partial_{\phi_{13}}\kappa_{1,3})\sigma^N_{1,2}I^J_{1,2}]/[(\partial_{\phi_{12}}\kappa_{1,2})\sigma^N_{1,3}I^J_{1,3}]$ in Fig. 7 where the scattering matrix at the junction is given in Eqs. (33)–(36). It is clear from the plot that there is a large deviation from our prediction for most of the parameter space in the case of nontopological superconductors. Here all the calculations for the Josephson current have been carried out using the Matsubara sum given in Eq. (37).

V. NOISE IN HEAT CURRENT

As our proposal involves the measurement of thermal conductance which in turn requires the measurement of heat current, it is important to understand the fluctuation in the heat current which if dominant can ruin the possibility of checking the validity of our predictions made in Eqs. (31) and (32). The noise in the heat current can be decomposed into equilibrium noise which will be dictated by the average temperature and will be consistent with the fluctuation-dissipation relation while the additional nonequilibrium noise is due to the finite temperature bias and the amplifier noise used to measure the noise itself. The amplifier noise will depend on the particulars of the experimental setup and is beyond the scope of our work. In the following sections we shall focus on the zero-frequency thermal noise for a two- and three-terminal Josephson junction.

A. Noise in heat current: Two-terminal case

For a two-terminal Josephson junction, the zero-frequency noise in heat current can be written as [72,73]

$$\begin{aligned} S^H(0) = \frac{1}{h}\sum_{\alpha\in\{e,h\}}\int_{\Delta_0}^{\infty} d\omega\,\omega^2\big(\mathcal{T}^{2,1}_\alpha\{f(\omega,T_1)[1-f(\omega,T_1)] \\ + f(\omega,T_2)[1-f(\omega,T_2)]\} \\ + \mathcal{T}^{2,1}_\alpha\big(1-\mathcal{T}^{2,1}_\alpha\big)[f(\omega,T_1)-f(\omega,T_2)]^2\big). \end{aligned} \tag{41}$$

The first two terms in the above equation correspond to the equilibrium noise, whereas the third term corresponds to shot noise which is finite only when $\mathcal{T}$ is different from unity or zero. The corresponding error in the heat current measured within a frequency bandwidth of $\Delta\mathtt{f}$ can be expressed as

$$\delta I^H = \sqrt{S^H(0)\Delta\mathtt{f}}. \tag{42}$$

We have calculated the percentage error $([(\delta I^H/I^H)/\sqrt{\Delta\mathtt{f}}])$ and plotted it for both nontopological and Majorana-Josephson junctions in Fig. 8 for lead temperatures $T_1 = 1.1$ K

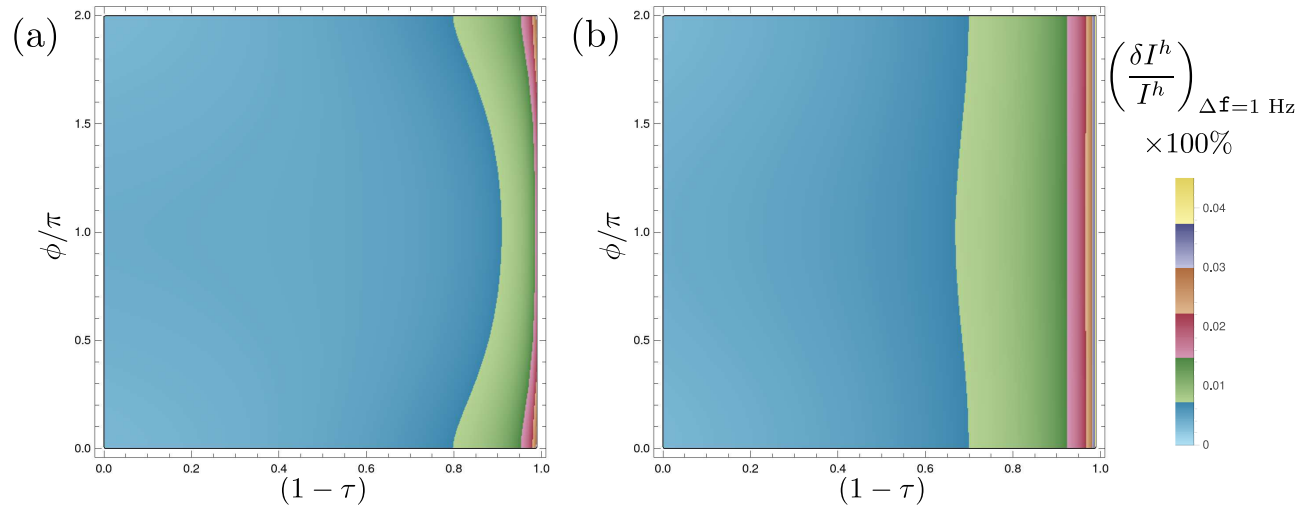

FIG. 8. Percentage error per $\sqrt{Hz}$ in the heat current for a Josephson junction with (a) quadratic dispersion and proximity-induced s-wave superconductivity and (b) helical edge state of quantum spin Hall state as a function of normal-state transmissivity τ and superconducting phase difference ϕ. Temperatures of left and right leads are assumed to be $T_1 = 1.1$ K and $T_2 = 0.9$ K, respectively. The superconducting pairing potential is assumed to be $\Delta_0 = 2k_B T_{\mathrm{avg}} \approx 172.347\ \mu$eV.

and $T_2 = 0.9$ K and superconducting pairing potential $\Delta_0 \approx 172.347\ \mu$eV in the parameter space (ϕ, τ). These parameter values are motivated from the experiments of Ref. [74]. As can be seen, the percentage fluctuation in the heat current stays reasonably small for a thermal bias which is of the same order as used in Ref. [74], hence we do not expect thermal noise to pose any serious hindrance to the experimental conformation of our result. At this point we would like to mention that the possibility of fluctuation of fermion parity [39] owing to the presence of fermion bath may lead to fluctuation of the Josephson current and hence can make the observation of Eq. (32) difficult but no such challenges are expected in the case of Eq. (31). This is due to the fact that the presence of the subgap bound state influences the thermal conductance directly but its occupancy does not unless Coulomb correlation plays an important role at the junction. Taking Coulomb correlation into account is beyond the scope of this paper. Also note that the fluctuation-dissipation relation obtained from Eq. (41) in the limit of zero thermal bias given by $S^H_{\mathrm{eq}}(0) = 2\kappa k_B T^2$ implies that equilibrium noise in heat current will depict an extra suppression for the case of a Majorana-Josephson junction as opposed to the nontopological Josephson junction owing to the results presented in Fig. 2 in the $\phi = 0$ limit.

General expression of zero-frequency noise for a three-terminal junction is algebraically lengthy to express in terms of the elements of the scattering matrix, superconducting phases, and the temperatures of the different leads. However, we have confirmed that in the case of a three-terminal junction, if one of the leads is kept at a temperature T_1 and the other two leads at temperature T_2, the expression of noise reduces to a form similar to the two-terminal result, Eq. (41). This indicates that even for a three-terminal case, the estimate of thermal noise in heat current will be of the same order of magnitude as it will be for the two-terminal junction and will continue to be small.

Hence, we conclude that the thermal noise generated in a realistic situation is not large enough to smear out the distinction between a Majorana and a non-Majorana Josephson junction predicted by us.

VI. DISCUSSION

In this paper we derived a set of two closed-form relations involving the thermal conductance, the Josephson current, and the normal-state electrical conductance for a three-terminal Josephson junction which emerge for the presence of a Majorana end state at the junction. We discussed our proposal in the context of a helical edge state of the quantum spin Hall state. In principle a similar proposal could also be discussed in the context of the nanowire setup [26–31,41,63,75] but this will be a more involved proposal which requires application of controlled magnetic fields on each wire forming the Josephson junction which will be explored in the future.

In general the signatures of the Majorana end state have been explored primarily for two perspectives: (a) the $2e^2/h$ conductance peak [29,76–80] and (b) the 4π Josephson effect [39,41,43]. Both the proposals exploit electrical current signals and they have their own caveats [59–63,81–84], hence it is important to explore new routes for looking for signatures of Majorana end states. Our approach puts heat and charge current measurements together such that the signature is neither based on observation of phase periodicity (like in the 4π effect) nor on an observation of a quantized tunnel conductance of $2e^2/h$. In particular, note that our first result [Eq. (31)] only depends on thermal conductance and normal-state electrical conductance of the junction and hence is independent of possible fluctuation of Josephson current owing to fermion parity fluctuations induced by fermionic bath coupled to the junction [39].

ACKNOWLEDGMENTS

A.M. acknowledges Ministry of Human Resource and Development, India for funding. S.D. acknowledges support from DST-SERB Grant No. MTR/2019/001043 and an ARF grant from IISER Kolkata.

APPENDIX A: TOTAL QUASIPARTICLE TRANSMISSION PROBABILITY FOR NONTOPOLOGICAL JOSEPHSON JUNCTION

For a nontopological two-terminal Josephson junction (s-wave superconductivity for 1D electrons with quadratic dispersion [4,5]), we have

$$\mathcal{T}_{ee}^{2,1} = \tau \frac{\left(\omega^2 - \Delta_0^2\right)\left(\omega^2 - \Delta_0^2 \cos^2\phi/2\right)}{\left[\omega^2 - \Delta_0^2(1 - \tau \sin^2\phi/2)\right]^2}, \tag{A1}$$

$$\mathcal{T}_{he}^{2,1} = \tau(1-\tau) \frac{\left(\omega^2 - \Delta_0^2\right)\left(\Delta_0^2 \sin^2\phi/2\right)}{\left[\omega^2 - \Delta_0^2(1 - \tau \sin^2\phi/2)\right]^2}, \tag{A2}$$

and $\mathcal{T}_e^{2,1} = \mathcal{T}_{ee}^{2,1} + \mathcal{T}_{he}^{2,1}$. Note that, at $\phi = 0$, $\mathcal{T}_{he}^{2,1} = 0$ and $\mathcal{T}_{ee}^{2,1} = \tau$ so that $\mathcal{T}_e^{2,1}(\phi = 0) = \tau$. We also have $\mathcal{T}_h^{2,1} = \mathcal{T}_e^{2,1}$ and thus at $\phi = 0$, $\mathcal{T}^{2,1} (= \mathcal{T}_e^{2,1} + \mathcal{T}_h^{2,1}) = 2\tau$.

APPENDIX B: THERMAL CONDUCTANCE, LANDAUER CONDUCTANCE, AND JOSEPHSON CURRENT OF A TOPOLOGICAL JOSEPHSON JUNCTION

The electrical conductance for a single channel of spinless electron with transmission probability τ is given by the Landauer formula [64,65,85]

$$\sigma^N = \frac{e^2\tau}{h}\beta(T) = \frac{e^2\tau}{h}\int_{-\infty}^{\infty}\left(-\frac{\partial f(\omega,T)}{\partial\omega}\right)d\omega = \frac{e^2\tau}{h}(4k_BT)^{-1}\int_{-\infty}^{\infty}\left[\cosh\left(\frac{\omega}{2k_BT}\right)\right]^{-2}d\omega, \tag{B1}$$

where e is the electronic charge and $f(\omega, T)$ is the Fermi distribution function at temperature T. Now, the thermal conductance can be expressed as [Eq. (2) in the main text]

$$\kappa(\phi) = \left[\frac{1}{h}\int_{\Delta_0}^{\infty} d\omega\, \omega \{\mathcal{T}^{2,1}\}\frac{\partial f(\omega,T)}{\partial T}\right]_{T=T_{\rm avg}}, \tag{B2}$$

where $T_{\rm avg}$ is the average junction temperature.

Now using (11),

$$\begin{aligned}\kappa &= \frac{2\tau}{h}\left[\int_{\Delta_0}^{\infty} d\omega\, \omega \frac{\omega^2 - \Delta_0^2}{\omega^2 - |\omega_0^{\pm}|^2}\frac{\partial f(\omega,T)}{\partial T}\right]_{T=T_{\rm avg}} \\ &= \sigma^N\left[\frac{2}{e^2\beta(T)}\int_{\Delta_0}^{\infty} d\omega\, \omega \frac{\omega^2 - \Delta_0^2}{\omega^2 - |\omega_0^{\pm}|^2}\frac{\partial f(\omega,T)}{\partial T}\right]_{T=T_{\rm avg}},\end{aligned} \tag{B3}$$

where we have used the expression (B1).

Again we know, the Josephson current (at temperature T) is given by [47]

$$I^J = I_1 + I_2 + I_3, \tag{B4}$$

$$I_1 = -\frac{2e}{\hbar}\frac{\partial|\omega_0^{\pm}|}{\partial\phi}\tanh\left(\frac{|\omega_0^{\pm}|}{2k_BT}\right), \tag{B5}$$

$$I_2 = -\frac{2e}{\hbar}2k_BT\int_{\Delta_0}^{\infty} d\omega \ln[\cosh(\omega/2k_BT)]\frac{\partial\rho(\omega,\phi)}{\partial\phi}, \tag{B6}$$

$$I_3 = \frac{2e}{\hbar}\frac{d}{d\phi}\int d\vec{r}|\Delta|^2/|g|, \tag{B7}$$

where g is the interaction constant of Bardeen-Cooper-Schrieffer theory. Here we have taken $|\Delta|$ to be independent of ϕ and hence the contribution from I_3 vanishes. I_2 is the contribution from the density of states $\rho(\omega, \phi)$ above the gap Δ_0, which also vanishes for short junction limit. Thus, $I^J = I_1$, i.e., the contribution from bound states alone. With this, we have

$$\begin{aligned}\frac{\partial\kappa}{\partial\phi} &= \frac{2\sigma^N}{e^2\beta(T)}\frac{\partial}{\partial\phi}\left[\int_{\Delta_0}^{\infty} d\omega\, \omega \frac{\omega^2 - \Delta_0^2}{\omega^2 - |\omega_0^{\pm}|^2}\frac{\partial f(\omega,T)}{\partial T}\right]_{T=T_{\rm avg}} \\ &= \frac{2\sigma^N}{e^2\beta(T)}\left[\int_{\Delta_0}^{\infty} d\omega\, \omega \frac{\omega^2 - \Delta_0^2}{(\omega^2 - |\omega_0^{\pm}|^2)^2}\frac{\partial f(\omega,T)}{\partial T}(-1)\left(-2|\omega_0^{\pm}|\frac{\partial|\omega_0^{\pm}|}{\partial\phi}\right)\right]_{T=T_{\rm avg}}\end{aligned}$$

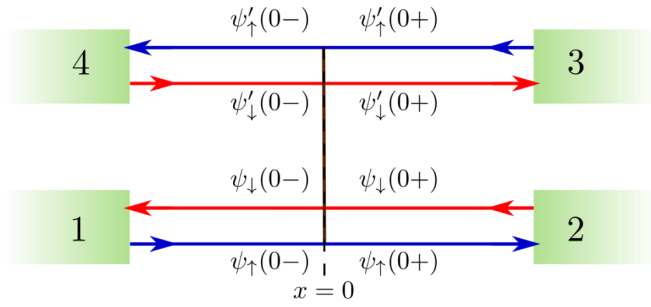

FIG. 9. Tunneling between the upper and lower edge with opposite helicity. The blue lines correspond to up spin while the red lines corresponds to down spin.

$$= \frac{2\sigma^N}{e^2\beta(T)}\left[\int_{\Delta_0}^{\infty} d\omega\,\omega\frac{\omega^2-\Delta_0^2}{(\omega^2-|\omega_0^{\pm}|^2)^2}\frac{\partial f(\omega,T)}{\partial T}(2|\omega_0^{\pm}|)\left\{-\frac{\hbar I^J}{2e}\coth\left(\frac{|\omega_0^{\pm}|}{2k_BT}\right)\right\}\right]_{T=T_{\rm avg}}$$

$$= \sigma^N I^J\left[\frac{-h|\omega_0^{\pm}|}{\pi e^3}\left\{\frac{1}{\beta(T)}\coth\left(\frac{|\omega_0^{\pm}|}{2k_BT}\right)\right\}\int_{\Delta_0}^{\infty} d\omega\,\omega\frac{\omega^2-\Delta_0^2}{(\omega^2-|\omega_0^{\pm}|^2)^2}\frac{\partial f(\omega,T)}{\partial T}\right]_{T=T_{\rm avg}}, \tag{B8}$$

which is Eq. (9), used in the main text.

APPENDIX C: 3 × 3 SCATTERING MATRIX FROM TUNNELING HAMILTONIAN

To derive the scattering matrix at $x = 0$, we first write the Hamiltonian ($\mathcal{H}$) as a sum of edge states Hamiltonian ($\mathcal{H}_{\rm edge}$) and tunneling Hamiltonian ($\mathcal{H}_T$) in second quantized notation.

$$\mathcal{H} = \mathcal{H}_{\rm edge} + \mathcal{H}_T, \tag{C1}$$

$$\mathcal{H}_{\rm edge} = \int dx\{\psi_\uparrow^\dagger(x)(-i\hbar v_F\partial_x-\mu)\psi_\uparrow(x)+\psi_\downarrow^\dagger(x)(i\hbar v_F\partial_x-\mu)\psi_\downarrow(x) + \psi_\uparrow'^\dagger(x)(i\hbar v_F\partial_x-\mu)\psi'_\uparrow(x)+\psi_\downarrow'^\dagger(x)(-i\hbar v_F\partial_x-\mu)\psi'_\downarrow(x)\}, \tag{C2}$$

$$\mathcal{H}_T = \hbar v_F\int dx\,\delta(x)\{s\,\psi_\uparrow^\dagger(x)\psi_\downarrow(x)+u\,\psi_\uparrow'^\dagger(x)\psi'_\downarrow(x)+t[\psi_\uparrow^\dagger(x)\psi'_\uparrow(x)+\psi_\downarrow^\dagger(x)\psi'_\downarrow(x)]+v[\psi_\uparrow^\dagger(x)\psi'_\downarrow(x)+\psi_\downarrow^\dagger(x)\psi'_\uparrow(x)]+\text{h.c.}\}. \tag{C3}$$

Here $\psi(x)$ and $\psi'(x)$ represents the lower edge (with helicity $\eta = 1$) and the upper edge (with helicity $\eta = -1$). For simplicity, we have assumed the parameters $\{s, t, u, v\}$ to be real. Apart from the overall factor of $\hbar v_F$, s and u are the backscattering amplitude in the lower and the upper edge, respectively. Interedge spin-conserving tunneling strength is given by t while the interedge spin-flip tunneling has strength v. Now we shall follow Ref. [86] to obtain the scattering matrix corresponding to the above given tunnel Hamiltonian. We note that $\psi'_\uparrow(0+)$, $\psi'_\downarrow(0-)$, $\psi_\downarrow(0+)$, and $\psi_\uparrow(0-)$ denote the incoming waves towards the junction, while $\psi'_\uparrow(0-)$, $\psi'_\downarrow(0+)$, $\psi_\downarrow(0-)$, and $\psi_\uparrow(0+)$ denote the outgoing waves from the junction (Fig. 9).

We represent the scattering matrix as

$$\begin{pmatrix}\psi_\downarrow(0-)\\ \psi_\uparrow(0+)\\ \psi'_\downarrow(0+)\\ \psi'_\uparrow(0-)\end{pmatrix} = \begin{pmatrix}S_{LR} & S_{LL} & S_{LL'} & S_{LR'}\\ S_{RR} & S_{RL} & S_{RL'} & S_{RR'}\\ S_{R'R} & S_{R'L} & S_{R'L'} & S_{R'R'}\\ S_{L'R} & S_{L'L} & S_{L'L'} & S_{L'R'}\end{pmatrix}\begin{pmatrix}\psi_\uparrow(0-)\\ \psi_\downarrow(0+)\\ \psi'_\uparrow(0+)\\ \psi'_\downarrow(0-)\end{pmatrix}, \tag{C4}$$

which readily defines the elements of S.

Now, using the relation

$$\lim_{\epsilon\to 0}\int_{-\epsilon}^{\epsilon} dx'\{\psi_\uparrow(x),\mathcal{H}\} = 0, \tag{C5}$$

we get

$$-i(S_{RR}-1)+\frac{s}{2}(S_{LR})+\frac{t}{2}(S_{L'R})+\frac{v}{2}(S_{R'R}) = 0, \tag{C6}$$

$$-i(S_{RL})+\frac{s}{2}(1+S_{LL})+\frac{t}{2}(S_{L'L})+\frac{v}{2}(S_{R'L}) = 0, \tag{C7}$$

$$-i(S_{RL'}) + \frac{s}{2}(S_{LL'}) + \frac{t}{2}(1 + S_{L'L'}) + \frac{v}{2}(S_{R'L'}) = 0, \tag{C8}$$

$$-i(S_{RR'}) + \frac{s}{2}(S_{LR'}) + \frac{t}{2}(S_{L'R'}) + \frac{v}{2}(1 + S_{R'R'}) = 0. \tag{C9}$$

Similarly, from

$$\lim_{\epsilon\to 0}\int_{-\epsilon}^{\epsilon} dx'\{\psi_{\downarrow}(x), \mathcal{H}\} = 0 \tag{C10}$$

we get

$$i(1 - S_{LL}) + \frac{s}{2}(S_{RL}) + \frac{t}{2}(S_{R'L}) + \frac{v}{2}(S_{L'L}) = 0, \tag{C11}$$

$$i(-S_{LR}) + \frac{s}{2}(S_{RR} + 1) + \frac{t}{2}(S_{R'R}) + \frac{v}{2}(S_{L'R}) = 0, \tag{C12}$$

$$i(-S_{LR'}) + \frac{s}{2}(S_{RR'}) + \frac{t}{2}(S_{R'R'} + 1) + \frac{v}{2}(S_{L'R'}) = 0, \tag{C13}$$

$$i(-S_{LL'}) + \frac{s}{2}(S_{RL'}) + \frac{t}{2}(S_{R'L'}) + \frac{v}{2}(S_{L'L'} + 1) = 0. \tag{C14}$$

Using

$$\lim_{\epsilon\to 0}\int_{-\epsilon}^{\epsilon} dx'\{\psi'_{\uparrow}(x), \mathcal{H}\} = 0 \tag{C15}$$

we get

$$i(1 - S_{L'L'}) + \frac{u}{2}(S_{R'L'}) + \frac{t}{2}(S_{RL'}) + \frac{v}{2}(S_{LL'}) = 0, \tag{C16}$$

$$i(-S_{L'R'}) + \frac{u}{2}(S_{R'R'} + 1) + \frac{t}{2}(S_{RR'}) + \frac{v}{2}(S_{LR'}) = 0, \tag{C17}$$

$$i(-S_{L'R}) + \frac{u}{2}(S_{R'R}) + \frac{t}{2}(S_{RR} + 1) + \frac{v}{2}(S_{LR}) = 0, \tag{C18}$$

$$i(-S_{L'L}) + \frac{u}{2}(S_{R'L}) + \frac{t}{2}(S_{RL}) + \frac{v}{2}(S_{LL} + 1) = 0. \tag{C19}$$

Using

$$\lim_{\epsilon\to 0}\int_{-\epsilon}^{\epsilon} dx'\{\psi'_{\downarrow}(x), \mathcal{H}\} = 0 \tag{C20}$$

we get

$$-i(S_{R'R'} - 1) + \frac{u}{2}(S_{L'R'}) + \frac{v}{2}(S_{RR'}) + \frac{t}{2}(S_{LR'}) = 0, \tag{C21}$$

$$-i(S_{R'L'}) + \frac{u}{2}(1 + S_{L'L'}) + \frac{v}{2}(S_{RL'}) + \frac{t}{2}(S_{LL'}) = 0, \tag{C22}$$

$$-i(S_{R'R}) + \frac{u}{2}(S_{L'R}) + \frac{v}{2}(S_{RR} + 1) + \frac{t}{2}(S_{LR}) = 0, \tag{C23}$$

$$-i(S_{R'L}) + \frac{u}{2}(S_{L'L}) + \frac{v}{2}(S_{RL}) + \frac{t}{2}(1 + S_{LL}) = 0. \tag{C24}$$

Solving the set of Eqs. (C6)–(C9), (C11)–(C14), (C16)–(C19), (C21)–(C24) scattering matrix elements S_{ij} can be obtained.

Now, due to the presence of a large Zeeman field perpendicular to the spin-polarization axis ($M\sigma_{\perp}$) applied locally on the helical edge corresponding to terminal 4, its spectrum will develop a gap leading to perfect back-reflection at the junction, i.e.,

$$\psi'_{\uparrow}(0-) = e^{i\delta}\,\psi'_{\downarrow}(0-), \tag{C25}$$

where δ is the phase associated with the back-reflection. This enables us to write an effective 3×3 scattering matrix within the terminals 1, 2, and 3 at $x = 0$ as

$$\begin{pmatrix} \psi_{\downarrow}(0-) \\ \psi_{\uparrow}(0+) \\ \psi'_{\downarrow}(0+) \end{pmatrix} = \begin{pmatrix} r_{11} & t_{12} & t_{13} \\ t_{21} & r_{22} & t_{23} \\ t_{31} & t_{32} & r_{33} \end{pmatrix} \begin{pmatrix} \psi_{\uparrow}(0-) \\ \psi_{\downarrow}(0+) \\ \psi'_{\uparrow}(0+) \end{pmatrix}. \tag{C26}$$

We define

$$S^e = \begin{pmatrix} r_{11} & t_{12} & t_{13} \\ t_{21} & r_{22} & t_{23} \\ t_{31} & t_{32} & r_{33} \end{pmatrix}. \tag{C27}$$

Here r_{ii} represents the amplitude of back-reflection within the terminal i and t_{ji} represents the amplitude of transmission from terminal i to terminal j. This matrix has the property $t_{ij} = t_{ji}$.

For completeness we write the explicit expressions as calculated,

$$r_{11} = \frac{16i(t^2 - su) - 4e^{i\delta}[s(4+u^2) - t(tu+4iv) - uv^2]}{e^{i\delta}[4i + s(2-iu) + 2u + i(t-v)^2][-4 - 2iu + s(-2i+u) - (t+v)^2] + 4[4u + s^2u - 4itv - s(t^2+v^2)]}, \tag{C28}$$

$$r_{22} = \frac{16i(su - v^2) + 4e^{i\delta}[s(4+u^2) - t(tu+4iv) - uv^2]}{ie^{i\delta}[-4 + 2iu + s(2i+u) - (t-v)^2][-4 - 2iu + s(-2i+u) - (t+v)^2] + 4[-4u - s^2u + 4itv + s(t^2+v^2)]}, \tag{C29}$$

$$r_{33} = \frac{16 + 4s^2 - 8t^2 + t^4 - 2st^2u + 4u^2 + s^2u^2 + 8istv - 8ituv - 8v^2 - 2t^2v^2 - 2suv^2 + v^4 - 4ie^{i\delta}[4u + s^2u - 4itv - s(t^2+v^2)]}{e^{i\delta}[-4 + 2iu + s(2i+u) - (t-v)^2][-4 - 2iu + s(-2i+u) - (t+v)^2] + 4i[4u + s^2u - 4itv - s(t^2+v^2)]}, \tag{C30}$$

$$t_{12} = -\frac{4i[-4u + s^2u - s(t^2+v^2)] + e^{i\delta}[-4(4+u^2) + s^2(4+u^2) + (t^2-v^2)^2 - 2s(t^2u + 4itv + uv^2)]}{e^{i\delta}[-4 + 2iu + s(2i+u) - (t-v)^2][-4 - 2iu + s(-2i+u) - (t+v)^2] + 4i[4u + s^2u - 4itv - s(t^2+v^2)]} = t_{21}, \tag{C31}$$

$$t_{13} = \frac{-16it + 4it^3 - 4istu - 8sv + 8uv - 4itv^2 + 4ie^{i\delta}[2it(s+u) + (-4 + t^2 + su)v - v^3]}{e^{i\delta}[-4 + 2iu + s(2i+u) - (t-v)^2][-4 - 2iu + s(-2i+u) - (t+v)^2] + 4i[4u + s^2u - 4itv - s(t^2+v^2)]} = t_{31}, \tag{C32}$$

$$t_{23} = \frac{8t(-s+u) - 4i(4 + t^2 + su)v + 4iv^3 - 4ie^{i\delta}[t^3 - 2i(s+u)v - t(-4 + su + v^2)]}{e^{i\delta}[-4 + 2iu + s(2i+u) - (t-v)^2][-4 - 2iu + s(-2i+u) - (t+v)^2] + 4i[4u + s^2u - 4itv - s(t^2+v^2)]} = t_{32}. \tag{C33}$$

The corresponding scattering matrix for hole S^h can be evaluated by exploiting particle-hole symmetry [87] and it turns out to be

$$S^h = \begin{pmatrix} -r_{11}^* & t_{12}^* & -t_{13}^* \\ t_{21}^* & -r_{22}^* & t_{23}^* \\ -t_{31}^* & t_{32}^* & -r_{33}^* \end{pmatrix}. \tag{C34}$$

The expression for S^h, obtained using particle-hole symmetry, can be understood as follows.

$$\Psi(x) = \sum_{\omega \geqslant 0} \varphi_\omega(x)\gamma_\omega + [\mathcal{C}\varphi_\omega](x)\gamma_\omega^\dagger, \tag{C35}$$

where $\Psi(x) = [\psi_{\uparrow(x)}, \psi_\downarrow(x), \psi_\downarrow^\dagger(x), -\psi_\uparrow^\dagger(x)]^T$ is expressed in Nambu notation in terms of field operators $\psi_{\uparrow(\downarrow)}$, $\varphi_\omega(x) = [u_{\omega,\uparrow}(x), u_{\omega,\downarrow}(x), v_{\omega,\downarrow}(x), v_{\omega,\uparrow}(x)]^T$ and the charge conjugation operator $\mathcal{C} = \mathcal{K}\tau_y \otimes \sigma_y$ with $\mathcal{K}$ being the complex conjugation. The operators $\gamma_\omega^\dagger$ and γ_ω are the creation and annihilation operators of a fermionic quasiparticle with energy ω, respectively.

From the fact that BdG Hamiltonian $\mathcal{H}_{\rm BdG}$ (which is assumed to be diagonal in the basis of $\gamma_\omega^\dagger$ and γ_ω) anticommutes with the charge conjugation operator $\mathcal{C}$ $[\{\mathcal{H}_{\rm BdG}, \mathcal{C}\} = 0]$, it is straightforward to show that if φ_ω is the solution of a BdG Hamiltonian $\mathcal{H}_{\rm BdG}$ with energy ω, then $[\mathcal{C}\varphi_\omega]$ will be the solution of the same Hamiltonian $\mathcal{H}_{\rm BdG}$ with energy $-\omega$. That implies that

$$\begin{pmatrix} u_{\omega,\uparrow}(x) \\ u_{\omega,\downarrow}(x) \\ v_{\omega,\downarrow}(x) \\ v_{\omega,\uparrow}(x) \end{pmatrix} = \begin{pmatrix} -v_{-\omega,\uparrow}^*(x) \\ v_{-\omega,\downarrow}^*(x) \\ u_{-\omega,\downarrow}^*(x) \\ -u_{-\omega,\uparrow}^*(x) \end{pmatrix}, \tag{C36}$$

which is used in obtaining the expression for S^h. In Eq. (C36), we have not explicitly put indices corresponding to the different leads but as expected this relation is individually true for each of the leads.

In this case, we have considered a scattering matrix which is independent of energy (ω). The full scattering matrix S can be written as

$$S = \begin{pmatrix} S^e & 0 \\ 0 & S^h \end{pmatrix} \tag{C37}$$

and it connects the coefficients u and v as below

$$\begin{pmatrix} u_\downarrow(0-) \\ u_\uparrow(0+) \\ u'_\downarrow(0+) \\ v_\downarrow(0-) \\ v_\uparrow(0+) \\ v'_\downarrow(0+) \end{pmatrix} = \begin{pmatrix} r_{11} & t_{12} & t_{13} & 0 & 0 & 0 \\ t_{21} & r_{22} & t_{23} & 0 & 0 & 0 \\ t_{31} & t_{32} & r_{33} & 0 & 0 & 0 \\ 0 & 0 & 0 & -r^*_{11} & t^*_{12} & -t^*_{13} \\ 0 & 0 & 0 & t^*_{21} & -r^*_{22} & t^*_{23} \\ 0 & 0 & 0 & -t^*_{31} & t^*_{32} & -r^*_{33} \end{pmatrix} \begin{pmatrix} u_\uparrow(0-) \\ u_\downarrow(0+) \\ u'_\uparrow(0+) \\ v_\uparrow(0-) \\ v_\downarrow(0+) \\ v'_\uparrow(0+) \end{pmatrix}. \tag{C38}$$

Note that we have suppressed the subscript ω as S is independent of energy. Now under the transformation

$$\begin{pmatrix} u_\uparrow(x) \\ u_\downarrow(x) \\ v_\downarrow(x) \\ v_\uparrow(x) \end{pmatrix} \to \begin{pmatrix} -v^*_\uparrow(x) \\ v^*_\downarrow(x) \\ u^*_\downarrow(x) \\ -u^*_\uparrow(x) \end{pmatrix}$$

[Eq. (C36)], the scattering matrix S remains invariant confirming the particle-hole symmetry of S.

APPENDIX D: PARAMETRIZATION OF THE 3 × 3 SCATTERING MATRIX

In the scattering matrix discussed in Appendix C, we put $s = 0$, $u = 0$, $\delta = 0$, $v = t$, then

$$r_{11} = r_{22} = -1 + \frac{1}{1+2t^2} = \frac{-2t^2}{1+2t^2} = -\left(\frac{2t^2}{1+2t^2}\right), \tag{D1}$$

$$r_{33} = -1 + \frac{2}{1+2t^2} = 2\left(\frac{-2t^2}{1+2t^2}\right) + 1 = 1 - 2\left(\frac{2t^2}{1+2t^2}\right), \tag{D2}$$

$$t_{12} = t_{21} = \frac{1}{1+2t^2} = \frac{1+2t^2-2t^2}{1+2t^2} = 1 - \left(\frac{2t^2}{1+2t^2}\right), \tag{D3}$$

$$t_{13} = t_{31} = t_{23} = t_{32} = -\frac{2it}{1+2t^2} = -i\left(\frac{2t}{1+2t^2}\right) = -i\sqrt{\frac{4t^2}{1+2t^2}}$$

$$= -i\sqrt{2\left(\frac{2t^2}{1+2t^2}\right)\left(1 - \frac{2t^2}{1+2t^2}\right)}. \tag{D4}$$

Now we note that, for any real number t, $0 \leqslant \frac{2t^2}{1+2t^2} \leqslant 1$. Thus, we can redefine $\frac{2t^2}{1+2t^2} = \lambda$ and hence we obtain

$$r_{11} = r_{22} = -\lambda, \tag{D5}$$

$$r_{33} = 1 - 2\lambda, \tag{D6}$$

$$t_{12} = t_{21} = 1 - \lambda, \tag{D7}$$

$$t_{13} = t_{31} = -i\sqrt{2\lambda(1-\lambda)} = t_{23} = t_{32}, \tag{D8}$$

where $0 \leqslant \lambda \leqslant 1$. Also note that this scattering matrix is symmetric between terminal 1 and terminal 2. We have used this parametrization in Secs. IV D and IV F of the main text.

APPENDIX E: THREE-TERMINAL JOSEPHSON JUNCTION WITH QUADRATIC DISPERSION AND *p*-WAVE SUPERCONDUCTIVITY

A Josephson junction based on 1D electrons with quadratic dispersion and proximity-induced p-wave superconductivity also hosts Majorana bound states. We consider the scattering matrix for electrons S^e at $x = 0$ to be of the same form as in (C27). In this case the scattering matrix for hole will be $S^h = S^{e*}$. Such junctions can be described using the BdG Hamiltonian [70]

$$\mathcal{H} = \left(-\frac{\hbar^2}{2m}\frac{\partial^2}{\partial x^2} - \mu\right)\tau_z - i\frac{\Delta(x)}{k_F}\frac{\partial}{\partial x}[\cos\phi_i\tau_x - \sin\phi_i\tau_y], \tag{E1}$$

where τ_n are the Pauli matrices acting on particle-hole basis; $\Delta(x) = \Delta_0\Theta(x-L)$ and ϕ_i is the superconducting phase of the ith superconducting lead (see Fig. 10).

For energies $\omega < \Delta_0$, the solutions in different regions can be written as

$$\Psi_{Si} = a_i \exp[i\kappa'_e x]\begin{pmatrix} e^{i\theta/2}e^{i\phi_{(2,3)}/2} \\ e^{-i\theta/2}e^{-i\phi_{(2,3)}/2} \end{pmatrix} + b_i \exp[-i\kappa'_h x]\begin{pmatrix} e^{-i\theta/2}e^{i\phi_{(2,3)}/2} \\ -e^{i\theta/2}e^{-i\phi_{(2,3)}/2} \end{pmatrix}, \tag{E2}$$

$$\Psi_{Ni} = p_i \exp[ik_e x]\begin{pmatrix} 1 \\ 0 \end{pmatrix} + q_i \exp[-ik_e x]\begin{pmatrix} 1 \\ 0 \end{pmatrix} + r_i \exp[ik_h x]\begin{pmatrix} 0 \\ 1 \end{pmatrix} + s_i \exp[-ik_h x]\begin{pmatrix} 0 \\ 1 \end{pmatrix}, \tag{E3}$$

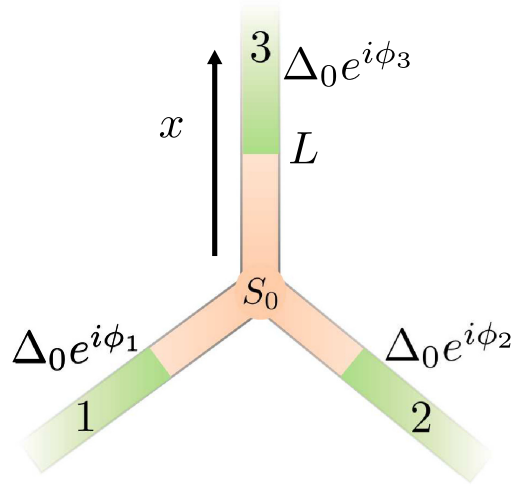

FIG. 10. Pictorial representation of a three-terminal Josephson junction based on 1D electrons with quadratic dispersion and with p-wave superconductivity. The coordinate system is chosen in such a way that $x = 0$ at the junction of the three terminals and increases in the direction of superconducting leads.

where $\theta = \arccos(\omega/\Delta_0)$. The subscripts $S(N)i$ denote superconducting (normal) region in the ith ($i \in \{1, 2, 3\}$) terminal. We consider the limit where owing to high doping limit ($\mu \gg \Delta_0, k_B T_{\rm avg}$) $\kappa_e' \simeq \kappa_h' \simeq k_e \simeq k_h \simeq k_F = (\sqrt{2m\mu})/\hbar$.

By demanding the continuity of the wave functions and their first derivatives across the boundaries and assuming that the amplitudes of the incoming and outgoing waves are related at $x = 0$ by the scattering matrices S^e and $S^h = S^{e*}$ we get the condition for bound state

$$\det[\mathbb{I} - a^2(\omega) S^e (-e^{i\Phi}) S^h e^{-i\Phi}] = 0, \tag{E4}$$

where $a(\omega) = (\frac{\omega}{\Delta_0} - i\frac{\sqrt{\Delta_0^2-\omega^2}}{\Delta_0})$ and Φ is the diagonal matrix with diagonal elements $\{\phi_1, \phi_2, \phi_3\}$.

This gives the bound state energies ω_0 and are given by $\omega = \omega_0^0, \omega_0^{\pm}$ [57] where

$$\omega_0^0 = 0, \tag{E5}$$

$$\omega_0^{\pm} = \pm\Delta_0 \sqrt{\tau_{12}\sin^2\frac{\phi_{12}}{2} + \tau_{13}\sin^2\frac{\phi_{13}}{2} + \tau_{23}\sin^2\frac{\phi_{23}}{2}} \tag{E6}$$

[$\phi_{ij} = \phi_j - \phi_i$; $\tau_{ij} = |t_{ij}|^2$].

For energies $\omega > \Delta_0$, we can calculate the total quasiparticle tunneling probability ($\mathcal{T}^{i,j}$) from terminal i to terminal j. We first consider an electronlike quasiparticle incident on the first superconducting lead. It will give rise to a reflected electronlike and holelike quasiparticle within the same lead with amplitudes, say, r_{ee} and r_{he}, respectively, and transmitted electronlike and holelike quasiparticles in superconducting nth lead with amplitudes, say, $t_{ee}^{n,1}$ and $t_{he}^{n,1}$, respectively. The wave functions can be written as

$$\Psi_{S1} = \exp[-i\kappa_e x]\begin{pmatrix} e^{\theta/2}e^{i\phi_1/2} \\ -e^{-\theta/2}e^{-i\phi_1/2}\end{pmatrix} + r_{ee}\exp[i\kappa_e x]\begin{pmatrix} e^{\theta/2}e^{i\phi_1/2} \\ e^{-\theta/2}e^{-i\phi_1/2}\end{pmatrix} + r_{he}\exp[-i\kappa_h x]\begin{pmatrix} e^{-\theta/2}e^{i\phi_1/2} \\ -e^{\theta/2}e^{-i\phi_1/2}\end{pmatrix}, \tag{E7}$$

$$\Psi_{S(2,3)} = t_{ee}^{(2,3),1}\exp[i\kappa_e x]\begin{pmatrix} e^{\theta/2}e^{i\phi_{(2,3)}/2} \\ e^{-\theta/2}e^{-i\phi_{(2,3)}/2}\end{pmatrix} + t_{he}^{(2,3),1}\exp[-i\kappa_h x]\begin{pmatrix} e^{-\theta/2}e^{i\phi_{(2,3)}/2} \\ -e^{\theta/2}e^{-i\phi_{(2,3)}/2}\end{pmatrix}, \tag{E8}$$

$$\Psi_{Ni} = p_i\exp[ik_e x]\begin{pmatrix}1\\0\end{pmatrix} + q_i\exp[-ik_e x]\begin{pmatrix}1\\0\end{pmatrix} + r_i\exp[ik_h x]\begin{pmatrix}0\\1\end{pmatrix} + s_i\exp[-ik_h x]\begin{pmatrix}0\\1\end{pmatrix}, \tag{E9}$$

where $\theta = \operatorname{arccosh}(\omega/\Delta_0)$. The subscripts $S(N)i$ denote superconducting (normal) region in the ith ($i \in \{1, 2, 3\}$) terminal.

From the continuity of the wave functions and their first derivatives and using the scattering matrices S^e and $S^h = S^{e*}$ we evaluate the values of $t_{ee}^{2,1}$, $t_{he}^{2,1}$, $t_{ee}^{3,1}$ and $t_{he}^{3,1}$. From these, we calculate

$$\mathcal{T}_e^{2,1} = \left|t_{ee}^{2,1}\right|^2 + \left|t_{he}^{2,1}\right|^2 = \frac{\tau_{12}\,\omega^2\left(\omega^2-\Delta_0^2\right)\left(\omega^2-|\omega_0^{\pm}|^2\right)}{\omega^2(\omega^2-|\omega_0^{\pm}|^2)^2} = \frac{\tau_{12}\,\omega^2\left(\omega^2-\Delta_0^2\right)\left(\omega^2-|\omega_0^{\pm}|^2\right)}{\prod_{\omega_0}(\omega-\omega_0)^2}, \tag{E10}$$

$$\mathcal{T}_e^{3,1} = \left|t_{ee}^{3,1}\right|^2 + \left|t_{he}^{3,1}\right|^2 = \frac{\tau_{13}\,\omega^2\left(\omega^2-\Delta_0^2\right)\left(\omega^2-|\omega_0^{\pm}|^2\right)}{\omega^2(\omega^2-|\omega_0^{\pm}|^2)^2} = \frac{\tau_{13}\,\omega^2\left(\omega^2-\Delta_0^2\right)\left(\omega^2-|\omega_0^{\pm}|^2\right)}{\prod_{\omega_0}(\omega-\omega_0)^2}, \tag{E11}$$

where $\omega_0^{\pm} = \pm\Delta_0\sqrt{\tau_{12}\sin^2\frac{\phi_{12}}{2} + \tau_{13}\sin^2\frac{\phi_{13}}{2} + \tau_{23}\sin^2\frac{\phi_{23}}{2}i^0}$ and ($\phi_{ij} = \phi_j - \phi_i$).

Similarly, for a holelike quasiparticle incident on the first superconducting lead we can calculate $t_{eh}^{2,1}$, $t_{hh}^{2,1}$, $t_{eh}^{3,1}$ and $t_{hh}^{3,1}$ and can define

$$\mathcal{T}_h^{2,1} = \left|t_{hh}^{2,1}\right|^2 + \left|t_{eh}^{2,1}\right|^2, \tag{E12}$$

$$\mathcal{T}_h^{3,1} = \left|t_{hh}^{3,1}\right|^2 + \left|t_{eh}^{3,1}\right|^2. \tag{E13}$$

As expected we have that $\mathcal{T}_h^{2,1} = \mathcal{T}_e^{2,1}$ and $\mathcal{T}_h^{3,1} = \mathcal{T}_e^{3,1}$ and thus

$$\mathcal{T}^{2,1} = \mathcal{T}_h^{2,1} + \mathcal{T}_e^{2,1} = 2\frac{\tau_{12}\left(\omega^2 - \Delta_0^2\right)}{\omega^2 - |\omega_0^{\pm}|^2}, \tag{E14}$$

$$\mathcal{T}^{3,1} = \mathcal{T}_h^{3,1} + \mathcal{T}_e^{3,1} = 2\frac{\tau_{13}\left(\omega^2 - \Delta_0^2\right)}{\omega^2 - |\omega_0^{\pm}|^2}. \tag{E15}$$

Similarly one can calculate $\mathcal{T}^{1,2}$, $\mathcal{T}^{3,2}$, $\mathcal{T}^{1,3}$, and $\mathcal{T}^{2,3}$. As our scattering matrix represents ($\tau_{ij} = \tau_{ji}$), hence $\mathcal{T}^{i,j} = \mathcal{T}^{j,i}$. It can be easily shown that $\mathcal{T}^{i,j}$ can be written in general as

$$\mathcal{T}^{i,j} = 2\frac{\tau_{ij}\,\omega^2\left(\omega^2 - \Delta_0^2\right)\left(\omega^2 - |\omega_0^{\pm}|^2\right)}{\prod_{\omega_0}(\omega - \omega_0)^2} = 2\frac{\tau_{ij}\left(\omega^2 - \Delta_0^2\right)}{\omega^2 - |\omega_0^{\pm}|^2}. \tag{E16}$$

These expressions are same as that derived in Sec. IV A of the main text, which justifies the fact that the central results of our paper, i.e., Eqs. (31) and (32) of the main text are not only true for a three-terminal Josephson junction based on a Dirac type spectrum of helical edge states but also for a three-terminal Josephson junction made out of 1D electrons with quadratic dispersion and proximity-induced p-wave superconductivity.

[1] K. Maki and A. Griffin, Phys. Rev. Lett. **15**, 921 (1965).
[2] K. Maki and A. Griffin, Phys. Rev. Lett. **16**, 258 (1966).
[3] G. D. Guttman, B. Nathanson, E. Ben-Jacob, and D. J. Bergman, Phys. Rev. B **55**, 3849 (1997).
[4] E. Zhao, T. Löfwander, and J. A. Sauls, Phys. Rev. Lett. **91**, 077003 (2003).
[5] E. Zhao, T. Löfwander, and J. A. Sauls, Phys. Rev. B **69**, 134503 (2004).
[6] A. Fornieri, G. Timossi, P. Virtanen, P. Solinas, and F. Giazotto, Nat. Nanotechnol. **12**, 425 (2017).
[7] X. Luo, Y. Peng, H. Shen, and X. Yi, Sci. Rep. **9**, 2187 (2019).
[8] B. Sothmann and E. M. Hankiewicz, Phys. Rev. B **94**, 081407(R) (2016).
[9] B. Sothmann, F. Giazotto, and E. M. Hankiewicz, New J. Phys. **19**, 023056 (2017).
[10] F. Giazotto and M. J. Martínez-Pérez, Nature (London) **492**, 401 (2012).
[11] D. Golubev, T. Faivre, and J. P. Pekola, Phys. Rev. B **87**, 094522 (2013).
[12] M. Martínez-Pérez and F. Giazotto, Appl. Phys. Lett. **102**, 182602 (2013).
[13] M. J. Martínez-Pérez, P. Solinas, and F. Giazotto, J. Low Temp. Phys. **175**, 813 (2014).
[14] M. J. Martínez-Pérez and F. Giazotto, Nat. Commun. **5**, 3579 (2014).
[15] M. J. Martínez-Pérez, A. Fornieri, and F. Giazotto, Nat. Nanotechnol. **10**, 303 (2015).
[16] A. Fornieri, C. Blanc, R. Bosisio, S. D'ambrosio, and F. Giazotto, Nat. Nanotechnol. **11**, 258 (2016).
[17] S. Kolenda, M. J. Wolf, and D. Beckmann, Phys. Rev. Lett. **116**, 097001 (2016).
[18] A. Fornieri, G. Timossi, R. Bosisio, P. Solinas, and F. Giazotto, Phys. Rev. B **93**, 134508 (2016).
[19] K. Y. Tan, M. Partanen, R. E. Lake, J. Govenius, S. Masuda, and M. Möttönen, Nat. Commun. **8**, 15189 (2017).
[20] A. Fornieri and F. Giazotto, Nat. Nanotechnol. **12**, 944 (2017).
[21] F. Paolucci, G. Marchegiani, E. Strambini, and F. Giazotto, Phys. Rev. Appl. **10**, 024003 (2018).
[22] B. Karimi and J. P. Pekola, Phys. Rev. Appl. **10**, 054048 (2018).
[23] M. König, H. Buhmann, L. W. Molenkamp, T. Hughes, C.-X. Liu, X.-L. Qi, and S.-C. Zhang, J. Phys. Soc. Jpn. **77**, 031007 (2008).
[24] R. M. Lutchyn, J. D. Sau, and S. Das Sarma, Phys. Rev. Lett. **105**, 077001 (2010).
[25] Y. Oreg, G. Refael, and F. von Oppen, Phys. Rev. Lett. **105**, 177002 (2010).
[26] S. Nadj-Perge, S. Frolov, E. Bakkers, and L. P. Kouwenhoven, Nature (London) **468**, 1084 (2010).
[27] D. Liang and X. P. Gao, Nano Lett. **12**, 3263 (2012).
[28] V. Mourik, K. Zuo, S. M. Frolov, S. R. Plissard, E. P. A. M. Bakkers, and L. P. Kouwenhoven, Science **336**, 1003 (2012).
[29] A. Das, Y. Ronen, Y. Most, Y. Oreg, M. Heiblum, and H. Shtrikman, Nat. Phys. **8**, 887 (2012).
[30] J. E. Sestoft, T. Kanne, A. N. Gejl, M. von Soosten, J. S. Yodh, D. Sherman, B. Tarasinski, M. Wimmer, E. Johnson, M. Deng *et al.*, Phys. Rev. Mater. **2**, 044202 (2018).
[31] J. D. S. Bommer, H. Zhang, O. Gül, B. Nijholt, M. Wimmer, F. N. Rybakov, J. Garaud, D. Rodic, E. Babaev, M. Troyer *et al.*, Phys. Rev. Lett. **122**, 187702 (2019).
[32] M. König, S. Wiedmann, C. Brüne, A. Roth, H. Buhmann, L. W. Molenkamp, X.-L. Qi, and S.-C. Zhang, Science **318**, 766 (2007).

[33] C. Brüne, A. Roth, E. G. Novik, M. König, H. Buhmann, E. M. Hankiewicz, W. Hanke, J. Sinova, and L. W. Molenkamp, Nat. Phys. **6**, 448 (2010).

[34] I. Knez, R.-R. Du, and G. Sullivan, Phys. Rev. Lett. **107**, 136603 (2011).

[35] C. Brüne, A. Roth, H. Buhmann, E. M. Hankiewicz, L. W. Molenkamp, J. Maciejko, X.-L. Qi, and S.-C. Zhang, Nat. Phys. **8**, 485 (2012).

[36] I. Knez, R.-R. Du, and G. Sullivan, Phys. Rev. Lett. **109**, 186603 (2012).

[37] S. Hart, H. Ren, T. Wagner, P. Leubner, M. Mühlbauer, C. Brüne, H. Buhmann, L. W. Molenkamp, and A. Yacoby, Nat. Phys. **10**, 638 (2014).

[38] A. Y. Kitaev, Phys. Usp. **44**, 131 (2001).

[39] L. Fu and C. L. Kane, Phys. Rev. B **79**, 161408(R) (2009).

[40] J. Nilsson, A. R. Akhmerov, and C. W. J. Beenakker, Phys. Rev. Lett. **101**, 120403 (2008).

[41] D. Laroche, D. Bouman, D. J. van Woerkom, A. Proutski, C. Murthy, D. I. Pikulin, C. Nayak, R. J. van Gulik, J. Nygård, P. Krogstrup *et al.*, Nat. Commun. **10**, 245 (2019).

[42] E. Bocquillon, R. S. Deacon, J. Wiedenmann, P. Leubner, T. M. Klapwijk, C. Brüne, K. Ishibashi, H. Buhmann, and L. W. Molenkamp, Nat. Nanotechnol. **12**, 137 (2017).

[43] H.-J. Kwon, K. Sengupta, and V. M. Yakovenko, Eur. Phys. J. B **37**, 349 (2004).

[44] S. S. Pershoguba and L. I. Glazman, Phys. Rev. B **99**, 134514 (2019).

[45] G. D. Guttman, E. Ben-Jacob, and D. J. Bergman, Phys. Rev. B **57**, 2717 (1998).

[46] J. A. Sauls, Phil. Trans. R. Soc. A **376**, 20180140 (2018).

[47] C. W. J. Beenakker, Phys. Rev. Lett. **67**, 3836 (1991).

[48] M. Octavio, M. Tinkham, G. E. Blonder, and T. M. Klapwijk, Phys. Rev. B **27**, 6739 (1983).

[49] J. Bardeen, R. Kümmel, A. E. Jacobs, and L. Tewordt, Phys. Rev. **187**, 556 (1969).

[50] P. Marra and M. Nitta, Phys. Rev. B **100**, 220502(R) (2019).

[51] G. Yang, Z. Lyu, J. Wang, J. Ying, X. Zhang, J. Shen, G. Liu, J. Fan, Z. Ji, X. Jing *et al.*, Phys. Rev. B **100**, 180501(R) (2019).

[52] G. V. Graziano, J. S. Lee, M. Pendharkar, C. Palmstrøm, and V. S. Pribiag, Phys. Rev. B **101**, 054510 (2020).

[53] This is so because each topological superconductor will contribute a single Majorana to the Josephson trijunction but two of them will hybridize and gap out while the third MES will stay topologically protected. Of course, it is assumed that each of the three 1D topological superconductors which form the trijunction are long enough so that the other three partner MESs formed at the ends of the wire which are opposite to the ones participating at the junction do not hybridize with their respective partners.

[54] P.-G. De Gennes, *Superconductivity of Metals and Alloys* (CRC, Boca Raton, FL, 2018).

[55] F. Dolcini, M. Houzet, and J. S. Meyer, Phys. Rev. B **92**, 035428 (2015).

[56] L. Fu and C. L. Kane, Phys. Rev. Lett. **100**, 096407 (2008).

[57] O. Deb, K. Sengupta, and D. Sen, Phys. Rev. B **97**, 174518 (2018).

[58] A. G. Bauer and B. Sothmann, Phys. Rev. B **99**, 214508 (2019).

[59] C.-X. Liu, J. D. Sau, T. D. Stanescu, and S. Das Sarma, Phys. Rev. B **96**, 075161 (2017).

[60] C.-X. Liu, J. D. Sau, and S. Das Sarma, Phys. Rev. B **97**, 214502 (2018).

[61] C. Moore, T. D. Stanescu, and S. Tewari, Phys. Rev. B **97**, 165302 (2018).

[62] C. Moore, C. Zeng, T. D. Stanescu, and S. Tewari, Phys. Rev. B **98**, 155314 (2018).

[63] O. A. Awoga, J. Cayao, and A. M. Black-Schaffer, Phys. Rev. Lett. **123**, 117001 (2019).

[64] R. Landauer, IBM J. Res. Dev. **1**, 223 (1957).

[65] M. Moskalets, *Scattering Matrix Approach to Non-Stationary Quantum Transport* (Imperial College Press, London, 2011), Chap. 1, pp. 1–33.

[66] If $\arg(S)_{i,j} \neq \arg(S)_{j,i}$ then the relative phase of the scattering matrix leads to an additive contribution to $\phi_{i,j}$ leading to anomalous Josephson current.

[67] J. Alicea, Rep. Prog. Phys. **75**, 076501 (2012).

[68] M. Houzet and J. S. Meyer, Phys. Rev. B **100**, 014521 (2019).

[69] P. Brouwer and C. Beenakker, Chaos, Solitons Fractals **8**, 1249 (1997).

[70] M. Thakurathi, O. Deb, and D. Sen, J. Phys.: Condens. Matter **27**, 275702 (2015).

[71] The following scattering matrix has been obtained using the command `RandomVariate[CircularOrthogonalMatrixDistribution[3]]` in Wolfram *Mathematica* 11.3.0.

[72] Y. Blanter and M. Büttiker, Phys. Rep. **336**, 1 (2000).

[73] P. Virtanen and F. Giazotto, AIP Adv. **5**, 027140 (2015).

[74] T. Faivre, D. Golubev, and J. P. Pekola, J. Appl. Phys. **116**, 094302 (2014).

[75] J. Cayao, A. M. Black-Schaffer, E. Prada, and R. Aguado, Beilstein J. Nanotechnol. **9**, 1339 (2018).

[76] A. R. Akhmerov, J. P. Dahlhaus, F. Hassler, M. Wimmer, and C. W. J. Beenakker, Phys. Rev. Lett. **106**, 057001 (2011).

[77] J. Liu, A. C. Potter, K. T. Law, and P. A. Lee, Phys. Rev. Lett. **109**, 267002 (2012).

[78] C.-H. Lin, J. D. Sau, and S. Das Sarma, Phys. Rev. B **86**, 224511 (2012).

[79] Y. Peng, F. Pientka, Y. Vinkler-Aviv, L. I. Glazman, and F. von Oppen, Phys. Rev. Lett. **115**, 266804 (2015).

[80] H. Zhang, C.-X. Liu, S. Gazibegovic, D. Xu, J. A. Logan, G. Wang, N. Van Loo, J. D. Bommer, M. W. De Moor, D. Car *et al.*, Nature (London) **556**, 74 (2018).

[81] F. Domínguez, F. Hassler, and G. Platero, Phys. Rev. B **86**, 140503(R) (2012).

[82] D. I. Pikulin and Y. V. Nazarov, Phys. Rev. B **86**, 140504(R) (2012).

[83] M. Houzet, J. S. Meyer, D. M. Badiane, and L. I. Glazman, Phys. Rev. Lett. **111**, 046401 (2013).

[84] Y. Peng, F. Pientka, E. Berg, Y. Oreg, and F. von Oppen, Phys. Rev. B **94**, 085409 (2016).

[85] C. W. J. Beenakker, Phys. Rev. B **46**, 12841(R) (1992).

[86] D. Wadhawan, K. Roychowdhury, P. Mehta, and S. Das, Phys. Rev. B **98**, 155113 (2018).

[87] A. Calzona and B. Trauzettel, Phys. Rev. Research **1**, 033212 (2019).